JGR Biogeosciences

RESEARCH ARTICLE
10.1029/2019JG005254

Coupling Water Column and Sediment Biogeochemical Dynamics: Modeling Internal Phosphorus Loading, Climate Change Responses, and Mitigation Measures in Lake Vansjø, Norway

Igor Markelov[1], Raoul-Marie Couture[2], Rachele Fischer[3], Sigrid Haande[4], and Philippe Van Cappellen[1]

[1]Ecohydrology Research Group, University of Waterloo, Waterloo, Ontario, Canada, [2]Aquatic Geochemistry Group, Department of Chemistry, Laval University, Québec City, Québec, Canada, [3]Great Lakes Office, Ontario's Ministry of the Environment, Toronto, Ontario, Canada, [4]Ferskvannsøkologi, Norwegian Institute for Water Research, Oslo, Norway

Abstract We expanded the existing one-dimensional MyLake model by incorporating a vertically resolved sediment diagenesis module and developing a reaction network that seamlessly couples the water column and sediment biogeochemistry. The application of the MyLake-Sediment model to boreal Lake Vansjø illustrates the model's ability to reproduce daily water quality variables and predict sediment-water column exchange fluxes over a long historical period. In prognostic scenarios, we assessed the importance of sediment processes and the effects of various climatic and anthropogenic drivers on the lake's biogeochemistry and phytoplankton dynamics. First, MyLake-Sediment was used to simulate the potential impacts of increasing air temperature on algal growth and water quality. Second, the key role of ice cover in controlling water column mixing and biogeochemical cycles was analyzed in a series of scenarios that included a fully ice-free end-member. Third, in another end-member scenario P loading from the watershed to the lake was abruptly halted. The model results suggest that remobilization of legacy P stored in the bottom sediments could sustain the lake's primary productivity on a time scale of several centuries. Finally, while the majority of management practices to reduce excessive algal growth in lakes focus on reducing external P loads, other efforts rely on the addition of reactive materials that sequester P in the sediment. Therefore, we investigated the effectiveness of ferric iron additions in decreasing the dissolved phosphate efflux from the sediment and, consequently, limit phytoplankton growth in Lake Vansjø.

Key Points:
- MyLake-Sediment model couples P biogeochemical cycling in water column and bottom sediments
- Remobilization of sediment P could sustain Lake Vansjø primary production for several centuries
- Climate warming and changing ice coverage have cascading effects on internal P loading

Supporting Information:
- Supporting Information S1

Correspondence to:
R.-M. Couture,
raoul.couture@chm.ulaval.ca

Citation:
Markelov, I., Couture, R.-M., Fischer, R., Haande, S., & Van Cappellen, P. (2019). Coupling water column and sediment biogeochemical dynamics: Modeling internal phosphorus loading, climate change responses, and mitigation measures in Lake Vansjø, Norway. *Journal of Geophysical Research: Biogeosciences*, *124*, 3847–3866. https://doi.org/10.1029/2019JG005254

Received 18 MAY 2019
Accepted 6 NOV 2019
Accepted article online 28 NOV 2019
Published online 26 DEC 2019
Corrected 10 FEB 2020

This article was corrected on 10 FEB 2020. See the end of the full text for details.

Author Contributions
Conceptualization: Igor Markelov, Raoul-Marie Couture, Philippe Van Cappellen
Data curation: Igor Markelov, Sigrid Haande
Formal Analysis: Igor Markelov, Raoul-Marie Couture
(continued)

1. Introduction

Lakes play a crucial role in water supply, food production, recreation, and climate regulation (Franz et al., 2018; Mueller et al., 2016; Tranvik et al., 2009). During the last century, changing climate, intensified agriculture, and urbanization have been exerting increasing pressures on lake ecosystem functioning and services (Adrian et al., 2009; Carvalho et al., 2013; Shimoda et al., 2011). Rising air temperatures and nutrient loadings have direct effects on lake physical and ecological properties (Ludsin et al., 2001; Schmid et al., 2014; Stefan et al., 2001; Winder & Sommer, 2012; Woolway & Merchant, 2019). Air and water temperatures are the key controlling factors of lake thermal regimes (Dibike et al., 2011; Livingstone, 2008), ice characteristics (Couture et al., 2015; Magnuson et al., 2000), and ecosystem metabolism (Winder & Sommer, 2012; Yvon-Durocher et al., 2012). Along with the meteorological drivers, increased P loading degrades lake water quality by intensifying primary production, potentially resulting in nuisance algal blooms and deoxygenation of bottom waters (Carvalho et al., 2013; Smith et al., 1999). A fraction of particulate inorganic and organic P, either externally derived (allochthonous) or produced in the lake (autochthonous), ultimately settles at the sediment-water interface (SWI), where a host of early diagenetic processes cycles P, leading either to the return of dissolved P to the hypolimnion or to permanent burial in the sediments. The fate of deposited P is highly variable as it depends on many different physical, biological, and geochemical properties and processes of the sedimentary reservoir (Dittrich et al., 2009; Katsev & Dittrich, 2013; Xiong et al., 2019).

After decades of sustained external P inputs, lakes have been shown to accumulate legacy P and experience mobilization of P from the sediment (i.e., internal loading), a phenomenon extensively reviewed in the literature (e.g., Orihel et al., 2017). Internal P load is a significant concern for stakeholders due to continued

Funding Acquisition: Raoul-Marie Couture, Philippe Van Cappellen
Investigation: Igor Markelov, Raoul-Marie Couture, Rachel Fischer, Sigrid Haande
Investigation: Igor Markelov, Raoul-Marie Couture, Rachele Fischer, Sigrid Haande
Methodology: Igor Markelov, Raoul-Marie Couture, Rachele Fischer, Philippe Van Cappellen
Project Administration: Raoul-Marie Couture
Resources: Raoul-Marie Couture, Philippe Van Cappellen
Software: Igor Markelov, Raoul-Marie Couture
Supervision: Raoul-Marie Couture, Philippe Van Cappellen
Validation: Igor Markelov, Raoul-Marie Couture
Visualization: Igor Markelov
Writing - Original Draft: Igor Markelov, Raoul-Marie Couture
Writing - review & editing: Igor Markelov, Raoul-Marie Couture, Sigrid Haande, Philippe Van Cappellen

water quality deterioration, with associated social and economic costs, and despite measures put in place to reduce external P loads (Matisoff et al., 2016; Mueller et al., 2016). Therefore, a predictive understanding of nutrient cycles within lake systems, and internal P loads in particular, is a primary research focus for maintaining and restoring healthy lake ecosystems.

Process-oriented lake modeling is a useful tool for guiding and assessing long-term management and water governance strategies. The crucial requirement of such modeling is the ability to accurately represent biogeochemical cycles in lakes and their response to the external drivers. Such models often rely on the assumption of lateral homogeneity, suitable in a vertically stratified environment, and are thus underpinned by 1-D hydrodynamic simulations coupled with ecological and biogeochemical modules of appropriate complexity (Janssen et al., 2015). However, representation of sediment-water interactions is not a standard feature of lake models and is often greatly simplified (Mooij et al., 2011; Soetaert et al., 2000).

Lacustrine sediments are a hot spot of enhanced biological activity. Multiple studies stress the vital importance of early diagenetic processes in controlling internal P loading in a variety of lake systems (Amirbahman et al., 2012; James, 2017; Loh, 2013; Nurnberg et al., 2013). While early diagenetic models can capture the drivers and timing of P release from sediment (Katsev, 2017; Katsev & Dittrich, 2013; Katsev et al., 2006; Li et al., 2018; McCulloch et al., 2013), these detailed models are not routinely coupled to lake water column models (Janssen et al., 2015; Paraska et al., 2014; Robson, 2014). Computational expense; complexity; and, possibly, the underestimated importance of early diagenetic processes have led model designers to simplify interactions between the sediment and the overlying water. Empirical lake models have been developed for internal P loading (e.g., Schauser et al., 2006; Bryhn & Haakanson, 2007), but their generalization is unlikely as their applicability tends to be site-specific. Popular approaches to couple sediment processes to lake water column models have included the incorporation of an empirical bottom flux boundary (Schmid et al., 2017) and vertically integrated submodules (e.g., oxic and anoxic layers; Janssen et al., 2015; Matzinger et al., 2010; Mooij et al., 2011; Schmid et al., 2017). Several well-established lake models, such as FABM-PCLake (Hu et al., 2016), DYRESM-CAEDYM (Trolle et al., 2008), CE-QUAL-W2 (Zhang et al., 2015), GLM (Hipsey et al., 2017), and DELWAQ (Smits & van Beek, 2013), were built on variations of those approaches in order to represent sediment-water interactions.

Here, we build upon two existing Matlab-based models: MyLake, which focuses on the reactions of P (Saloranta & Andersen, 2007), oxygen (O; Couture et al., 2015), and carbon (C; de Wit et al., 2018; Kiuru et al., 2018), and Matsedlab, which focuses on the reactions of O, C, iron (Fe; Couture, Gobeil, et al., 2010), sulphur (S; Couture et al., 2016), and nitrogen (N; Akbarzadeh et al., 2018). In order to couple the two individual models into the 1.5-D Lake-Sediment model, we merged their reactions networks. The goal is to deliver an open-access tool for the combined modeling of water column and sediment that uses a coherent biogeochemical reaction network. Consequently, we updated Matsetlab with reactions of P, aluminum (Al), calcium (Ca), and MyLake with reactions of N, Fe, Al, Ca, and S (Ahlgren et al., 2011; Canavan et al., 2006; Couture, Shafei, et al., 2010; Dijkstra et al., 2018; Dittrich et al., 2009; Doan et al., 2018; Gudimov et al., 2016; Katsev & Dittrich, 2013; Katsev et al., 2006; Li et al., 2018; Parsons et al., 2017; Testa et al., 2013; Van Cappellen & Wang, 1996).

We evaluate the coupled Lake-Sediment model against measurements both as time series and as vertical profiles in the water column, the solid-phase sediment, and the sediment pore water of eutrophied Lake Vansjø in Norway. We simulate the responses to (1) variable climate (air temperature), (2) absence of ice cover, and (3) external P load cutoff. We further showcase the use of the model to assess a management practice aimed at reducing internal P loads via the addition of reactive Fe to the water column.

2. Model Formulation, Study Site, and Methods

2.1. Model Formulation

MyLake is a one-dimensional, process-based model that simulates daily vertical distributions of lake water temperature, density stratification, and mixing and accounts for seasonal lake ice and snow cover. It further represents simplified P-phytoplankton dynamics where growth is limited by temperature, light, and nutrient availability (Saloranta & Andersen, 2007). In the current study, the existing physical hydrodynamic, ice, and snow cover modules of MyLake were used, and the P-phytoplankton module was reformulated for direct coupling to the reaction network in the sediment. Biogeochemical reactions involving O (Couture et al.,

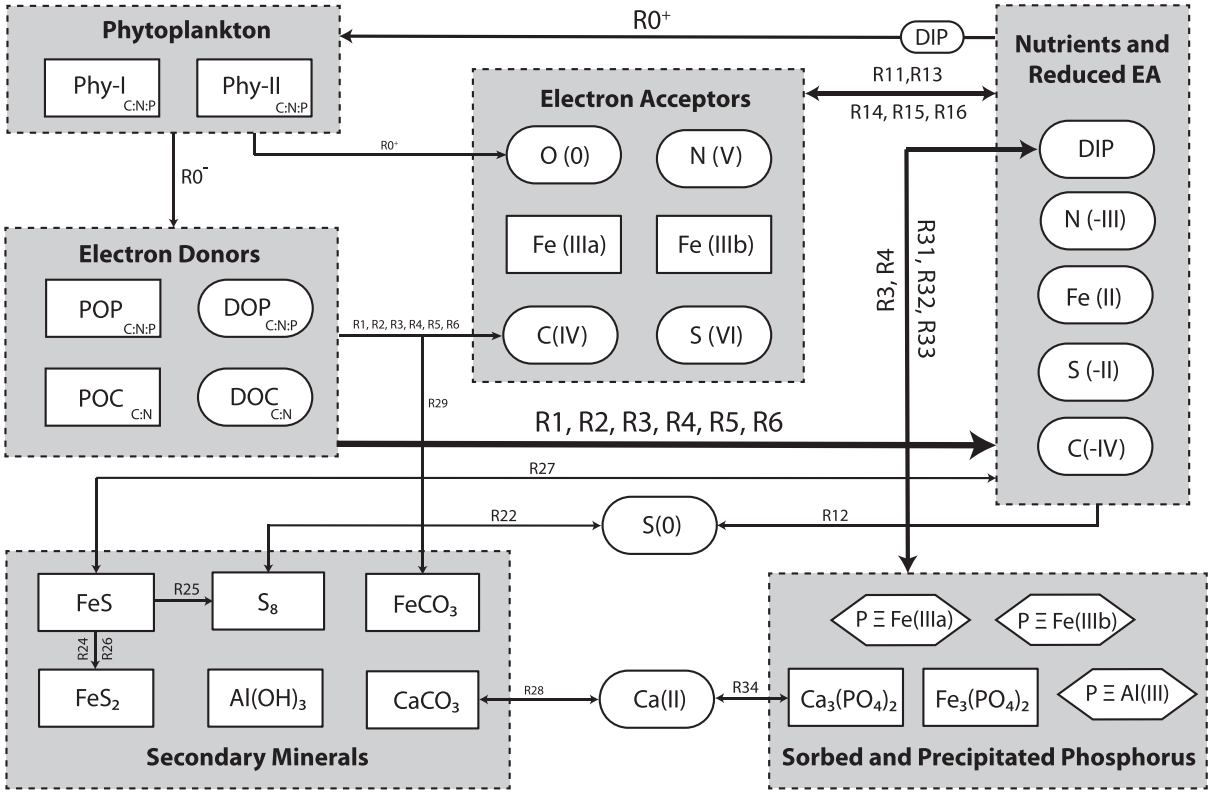

Figure 1. Reaction network for P, O, C, N, Fe, Al, Ca, and S in water column and sediment. Squared boxes represent particulate organic and mineral phases, rounded boxes represent aqueous species, and polygons represent P sorbed onto ferric Fe and Al (hydr)oxides.

2015) and C (de Wit et al., 2018; Kiuru et al., 2018), as well as reactions of N, Fe, Al, Ca, and S, were similarly coupled between sediment and water column (Figure 1; Tables 1 and 2).

The sediment module is a modified and adapted version of Matsetlab (Couture et al., 2016) rewritten specifically for coupling to the water column module. The mathematical representation of the sediment module consists of coupled nonlinear advection-diffusion-reaction equations, which represent reactive transport processes of solid and aqueous species in the sediment. Transport processes such as bioturbation, molecular diffusion, burial of solids, solute irrigation, and compaction are implemented according to Boudreau (1997). Finally, MATLAB's *pdepe* solver used in Matsedlab has been replaced by operator splitting algorithm with the Crank-Nicolson method for the transport step and Butcher's fifth-order Runge-Kutta method for the reaction step.

In addition to P, the continuous (i.e., in water column and sediment) reaction network takes into account the coupled cycles of key biogeochemical elements (O, C, N, Fe, Al, Ca, and S), which play important roles in controlling P cycling in the water column and sediments (Hadley et al., 2012; Iho et al., 2017; Lehtoranta et al., 2009; Verschoor et al., 2017). The model has been designed to study P partitioning among major P-binding forms commonly quantified by operational P-fractionation schemes (Doan et al., 2018). The reaction network includes microbially mediated primary and secondary redox reactions, aqueous speciation, mineral dissolution, and precipitation (Figure 1; Tables 1, 2, and S1). Microbially mediated organic matter degradation (i.e., aerobic respiration, denitrification, iron and sulfate reduction, and methanogenesis) is implemented using Michaelis-Menten rate laws. Bimolecular reaction rate laws are used for secondary redox reactions (e.g., oxidation of Fe^{2+}, NH_4^+, and HS^-), whereas precipitation and dissolution kinetics of the minerals depend on the corresponding degree of saturation and pH. In MyLake-Sediment, pH can be either (a) fixed by the user, as was done here, or calculated via (b) the electroneutrality equation, or (c) by calling a compiled version of PhreeqC (Parkhurst & Appelo, 2013). The majority of the reaction network parameters are set according to previous studies (Atkin & Tjoelker, 2003; Canavan et al., 2006; Couture et al., 2016; Dijkstra et al., 2018; Katsev & Dittrich, 2013; Parkhurst & Appelo, 2013; Van Cappellen & Wang, 1996), while

Table 1
Algal Dynamics and OM Degradation Reactions (Primary Reactions) Included in the MyLake-Sediment Model

No.	Reaction	Equation
Algae dynamics		
R0a	$(x - y + 2z)CO_2 + (y - 2\,z)HCO_3^- + yNH_4^+ + zHPO_4^{2-} + (x - y + 2z)H_2O \leftrightarrow (CH_2O)_x(NH_3)_y(H_3PO_4)_z + xO_2$	$\mu(20)Q_{10}^{(T-20)/10}[A]\frac{\lambda}{\epsilon_i \Delta z_i}\times \left[H\left(\frac{I'_{zi}}{I'}\right) - H\left(\frac{I'_{zi+1}}{I'}\right)\right]\times \frac{[HPO_4^{2-}]}{[HPO_4^{2-}]+P'}$
R0b	$(x + y + 2z)CO_2 + yNO_3^- + z\,HPO_4^{2-} + (x + 2y + 2z)H_2O \leftrightarrow (CH_2O)_x(NH_3)_y(H_3PO_4)_z + (y + 2\,z)HCO_3^- + (x + 2y + 2z)\,O_2$	$-m(20)Q_{10}^{(T-20)/10}[A]$
Primary redox reactions		
R1	$OM + x\,O_2 \rightarrow (x - y + 2z)CO_2 + (y - 2\,z)HCO_3^- + + yNH_4^+ + z\,HPO_4^{2-} + (x - y + 2z)H_2O$	
R2	$OM + 0.5\,x\,NO_3^- + (y - 2z)CO_2 + (0.5\,x + y - 2z)H_2O \rightarrow 0.5\,x\,N_2(g) + (x + y - 2\,z)\,HCO_3^- + yNH_4^+ + z\,HPO_4^{2-}$	$k(5)[OM]f_iQ_{10}^{(T-5)/10}$
R3	$OM + 4\,x\,Fe(OH)_3 + (7\,x + y - 2\,z)CO_2 \rightarrow 4\,x\,Fe^{2+} + (8x + y - 2z)HCO_3^- + yNH_4^+ + z\,HPO_4^{2-} + (3x - y + 2z)H_2O$	where
R4	$OM + 4\,x\,FeOOH + (7\,x + y - 2\,z)CO_2 + (x + y - 2z)H_2O \rightarrow 4\,x\,Fe^{2+} + (8x + y - 2z)HCO_3^- + yNH_4^+ + z\,HPO_4^{2-}$	$f_i = \frac{[EA]_i}{[EA]_i + K_{mi}^{EA}}\times$
R5	$OM + 0.5\,x\,SO_4^{2-} \rightarrow 0.5\,x\,HS^- + (0.5x - y + 2\,z)CO_2 + + (0.5x + y - 2z)HCO_3^- + yNH_4^+ + z\,HPO_4^{2-} + (0.5x - y + 2\,z)H_2O$	$\times\prod_{j=1}^{N-1}\frac{K_{mj}^{EA}}{[EA]_j + K_{mj}^{EA}}$
R6	$OM + (y - 2\,z)H_2O \rightarrow 0.5\,x\,CH_{4(aq)} + (0.5x - y + 2z)CO_2 + (y - 2z)HCO_3^- + yNH_4^+ + z\,HPO_4^{2-}$	

Note. OM = organic matter; x, y, and z define the C:N:P elemental composition of the organic matter produced or degraded in reactions R0-R6; $\mu(20)$ is the specific growth rate of algae at 20 ° C; Q_{10} is the Q_{10} temperature coefficient; $[A]$ is the concentration of algae; λ is the fractional day length; ϵ_i is the attenuation coefficient for layer i; Δz_i is the thickness of the layer i; H is the light limitation function (Saloranta & Andersen, 2007); I'_{zi} is the photosynthetically active irradiance at noon at the depth level z_i; I' is the light saturation level of photosynthesis P' is the limiting concentration of HPO_4^{2-}; $m(20)$ is the algae loss rate at 20 ° C; $k(5)$ is the degradation rate constant at 5 ° C; $[OM]$ is the concentration of organic matter (i.e., POP, DOP, POC, and DOC); $[EA]_i$ is the concentration of the electron acceptor (i.e., O_2, NO_3^-, $Fe(OH)_3$, FeOOH, and $SO4^{2-}$); K_{mi}^{EA} is the half-saturation constant. Parameter values used in the simulation are listed in Tables S2 and S4 in the supporting information.

others were either calibrated using the global optimization toolbox in MATLAB, which relies on a genetic algorithm, or manually fine-tuned to obtain the best overall fit to the observations.

Coupling of the water column and sediment across the SWI accounts for fluxes of dissolved and solid species. Each time step of the two-way coupled model involves the following three sequential operations: (i) MyLake provides boundary conditions for solid (Neumann type) and aqueous (Dirichlet type) species to the sediment module; (ii) results of the sediment module run are used to estimate the diffusive and nonlocal transport fluxes of dissolved species across the SWI; (iii) these fluxes across the SWI are used to update the concentrations of dissolved species in the benthic boundary layer of the water column; (iv) MyLake then proceeds to the next time step.

Specifically, MyLake provides boundary conditions for the sediment solid and aqueous species. The settling (advective) flux of a solid constituent from the water column to the sediment is proportional to its concentration in the water column C_i^s times its settling velocity w_s. Additionally, in the coupled model, significant accumulation of sediment is assumed to be restricted to water depths exceeding a user-specified "sediment effective depth" (Figure 2). Thus, for the solid s, the one-dimensional, sediment surface area-weighted deposition flux at the SWI is estimated as follows:

$$F_j^s = \sum_1^n \omega_s \cdot C_{i,j}^s \cdot \frac{A_i - A_{i-1}}{A_{sed}}, \quad (1)$$

Table 2
Secondary Redox Reactions, Mineral Precipitation-Dissolution Reactions, P Sorption and Precipitation Reactions, and Equilibrium Reactions in the Coupled MyLake-Sediment Model

No.	Reaction	Kinetic or equilibrium
Secondary redox reactions		
R11	$HS^- + 2O_2 \rightarrow H^+ + SO_4^{2-}$	$k_{tsox}[O_2][\sum S(-II)]$
R12	$HS^- + 2Fe(OH)_3 + 5H^+ \rightarrow 2Fe^{2+} + S(0) + 6H_2O$	$k_{tsfe}\,[Fe(OH)_3]\,[\sum S(-II)]$
R13	$Fe^{2+} + \frac{1}{4}O_2 + 2HCO_3^- + \frac{1}{2}H_2O \rightarrow Fe(OH)_3 + 2CO_2$	$k_{feox}\,[Fe^{2+}]\,[O_2]$
R14	$2O_2 + NH_4^+ + 2HCO_3^- \rightarrow NO_3^- + 2CO_2 + 3H_2O$	$k_{amox}\,[O_2]\,[NH_4^+]$
R15	$CH_4 + O_2 \rightarrow CO_2 + H_2O$	$k_{ch4o2}\,[CH_4]\,[O_2]$
R16	$CH_4 + SO_4^{2-} + CO_2 \rightarrow H_2S + 2HCO_3-$	$k_{ch4so4}\,[CH_4]\,[SO_4^{2-}]$
Mineral precipitation-dissolution reactions		
R21	$OM + HS^- \rightarrow OMS$	$k_{oms}\quad[\sum OM]\,[\sum S(-II)]$
R22a	$S(0) \rightarrow S_8$	$k_{spre}[S(0)]$
R22b	$S_8 \rightarrow S(0)$	$k_{sdis}\,[S_8]$
R23	$FeS_2 + 5O_2 + H^+ \rightarrow FeOOH + 2SO_4^{2-}$	$k_{fes2ox}\,[FeS_2]\,[O_2]$
R24	$FeS + S(0) \rightarrow FeS_2$	$k_{fespre}\,[FeS]\,[S(0)]$
R25	$4FeS + 3O_2 + 2H_2O \rightarrow 4S_8 + FeOOH$	$k_{fesox}\,[FeS]\,[O_2]$
R26	$FeS + HS^- + H^+ \rightarrow FeS_2 + H_2$	$k_{fes2pre}\,[FeS]\,[\sum S(-II)]$
R27a	$Fe^{2+} + HS^- \rightarrow FeS + H^+$	$k_{fepre}(\Omega_{FeS} - 1)$
R27b	$FeS + H^+ \rightarrow Fe^{2+} + HS^-$	$k_{fedis}\,[FeS]\,(1 - \Omega_{FeS})$
R28a	$Ca^{2+} + CO_3^{2-} \rightarrow CaCO_3$	$k_{CCpre}(\Omega_{CC} - 1)$
R28b	$CaCO_3 \rightarrow Ca^{2+} + CO_3^{2-}$	$k_{CCdis}\,[CaCO_3]\,(1 - \Omega_{CC})$
R29a	$Fe^{2+} + CO_3^{2-} \rightarrow FeCO_3$	$k_{FCpre}\,(\Omega_{FC} - 1)$
R29b	$FeCO_3 \rightarrow Fe^{2+} + CO_3^{2-}$	$k_{FCdis}\,[FeCO_3]\,(1 - \Omega_{FC})$
Phosphorus sorption and precipitation reactions		
R31a	$HPO_4^{2-} + Fe(OH)_3 \rightarrow PO_4 \equiv Fe(OH)_3 + H^+$	$k_{psorb}^{Fe(IIIa)}\,[Fe(OH)_3]\,[HPO_4^{2-}]$
R31b	$PO_4 \equiv Fe(OH)_3 + H^+ \rightarrow HPO_4^{2-} + Fe(OH)_3$	$4R3 + 2R12$
R32a	$HPO_4^{2-} + FeOOH \rightarrow PO_4 \equiv FeOOH + H^+$	$k_{psorb}^{Fe(IIIb)}[FeOOH]\,[HPO_4^{2-}]$
R32b	$PO_4 \equiv FeOOH + H^+ \rightarrow HPO_4^{2-} + FeOOH$	$4R4$
R33a	$3Fe^{2+} + 2HPO_4^{2-} \rightarrow Fe_3(PO_4)_2 + 2H^+$	$k_{Vpre}(\Omega_V - 1)$
R33b	$Fe_3(PO_4)_2 + 2H^+ \rightarrow 3Fe^{2+} + 2HPO_4^{2-}$	$k_{Vdis}\,[Fe_3(PO_4)_2]\,(1 - \Omega_V)$
R34a	$3Ca^{2+} + 2HPO_4^{2-} \rightarrow Ca_3(PO_4)_2 + 2H^+$	$k_{Apre}(\Omega_A - 1)$
R34b	$Ca_3(PO_4)_2 + 2H^+ \rightarrow 3Ca^{2+} + 2HPO_4^{2-}$	$k_{Adis}\,[Ca_3(PO_4)_2]\,(1 - \Omega_A)$
R35a	$HPO4^{2-} + Al(OH)_3 \rightarrow H^+ + PO_4 \equiv Al(OH)_3$	$k_{psorb}^{Al}\,[Al(OH)_3]\,[HPO_4^{2-}]$
Equilibrium reactions		
R31a	$HPO_4^{2-} + Fe(OH)_3 \rightarrow PO_4 \equiv Fe(OH)_3 + H^+$	$k_{psorb}^{Fe(IIIa)}\,[Fe(OH)_3]\,[HPO_4^{2-}]$
R31b	$PO_4 \equiv Fe(OH)_3 + H^+ \rightarrow HPO_4^{2-} + Fe(OH)_3$	$4R3 + 2R12$
R32a	$HPO_4^{2-} + FeOOH \rightarrow PO_4 \equiv FeOOH + H^+$	$k_{psorb}^{Fe(IIIb)}[FeOOH]\,[HPO_4^{2-}]$
R32b	$PO_4 \equiv FeOOH + H^+ \rightarrow HPO_4^{2-} + FeOOH$	$4R4$
R33a	$3Fe^{2+} + 2HPO_4^{2-} \rightarrow Fe_3(PO_4)_2 + 2H^+$	$k_{Vpre}(\Omega_V - 1)$
R33b	$Fe_3(PO_4)_2 + 2H^+ \rightarrow 3Fe^{2+} + 2HPO_4^{2-}$	$k_{Vdis}\,[Fe_3(PO_4)_2]\,(1 - \Omega_V)$
R34a	$3Ca^{2+} + 2HPO_4^{2-} \rightarrow Ca_3(PO_4)_2 + 2H^+$	$k_{Apre}(\Omega_A - 1)$
R34b	$Ca_3(PO_4)_2 + 2H^+ \rightarrow 3Ca^{2+} + 2HPO_4^{2-}$	$k_{Adis}\,[Ca_3(PO_4)_2]\,(1 - \Omega_A)$
R35a	$HPO4^{2-} + Al(OH)_3 \rightarrow H^+ + PO_4 \equiv Al(OH)_3$	$k_{psorb}^{Al}\,[Al(OH)_3]\,[HPO_4^{2-}]$

Table 2
Continued

No.	Reaction	Kinetic or equilibrium
Equilibrium reactions		
R41	$CO_{2(aq)} + H_2O = H_2CO_3 = HCO_3^- + H^+ = CO_3^{2-} + 2H^+$	$K_{C0}K_{C1}K_{C2}$
R42	$H_3PO_4 = H_2PO_4^- + H^+ = HPO_4^{2-} + 2H^+ = PO_4^{3-} + 3H^+$	$K_{P1}K_{P2}K_{P3}$
R43	$H_2S = HS^- + H^+$	K_{H_2S}
R44	$NH_4^+ = NH_3 + H^+$	K_{NH_4}
R45	$H_2O = H^+ + OH^-$	K_{H_2O}

Note. Two pools of Fe(III) are used to represent two pathways of Fe (oxy)hydroxide formation that yield minerals with different reactivities (Couture et al., 2016). The first pathway produces reactive $Fe(OH)_3$ upon oxidation of ferrous Fe (R13); the second pathway yields less reactive FeOOH through the oxidation of pyrite and mackinawite (R23, R25). Parameter values used in the simulation are listed in Table S4.

where spatial and temporal grids points are represented by indices i and j, respectively; ω_s is the settling velocity of the solid particles in the water column; $C^s_{i,j}$ is the concentration of the solid constituent in the water column; A_i is the area of the sediment below ith layer of water column; A_{i-1} is the area of the sediment below $(i-1)$th layer of water column; and A_{sed} is the total area of the sediment below the "sediment effective depth". The numbering of the layers starts at the deepest point of the lake with $A_0 = 0$. The sediment boundary condition for solute a is the area-weighted mean concentration in the water column below the "sediment effective depth":

$$C^a_j = \sum_1^n C^a_{i,j} \cdot \frac{A_i - A_{i-1}}{A_{sed}}. \tag{2}$$

Pore water profiles modeled in the sediment are used to estimate fluxes at the SWI. Thus, the flux of solute a at the SWI is estimated as the sum of diffusive and nonlocal bioirrigation fluxes:

$$F^a_j = -\frac{\varphi D^a_o}{\theta^2}\frac{\partial C^a_{i,j}}{\partial z} + \alpha \int_0^L (C^a_{i,j}(z) - C^a_{0,j})dz, \tag{3}$$

where φ is the porosity, D^a_o is the temperature corrected molecular diffusion coefficient of solute a, θ is the tortuosity, $C^a_{i,j}$ is the concentration of dissolved species, $C^a_{0,j}$ is the concentration of dissolved species at the SWI (i.e., bottom water concentration), z is depth in the sediment with $z = 0$ at the SWI, α is the irrigation coefficient, and L is the the depth of irrigation. The diffusive flux is estimated using a fourth-order finite-difference approximation. The integral is estimated using the trapezoidal method.

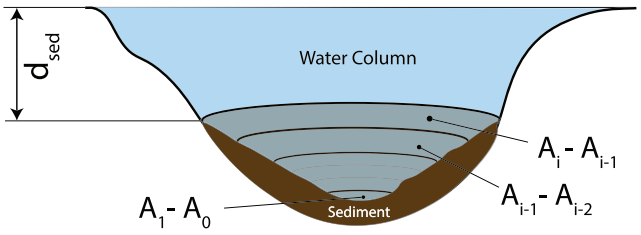

Figure 2. Representation of sediment in the model. Due to sediment focusing toward the deeper parts of the lake, significant accumulation of sediment is assumed to only occur below a user-defined "sediment effective depth," d_{sed}. If A_i is the surface area of the water column layer that intersects the SWI at depth d_{sed} and A_{i-1} that of the water column layer below it, then $A_i - A_{i-1}$ is the area of the SWI that captures the particulate matter deposited at water depth d_{sed} and across which solutes are exchanged between the sediment pore water and the ith water layer. The SWI is similarly divided until the lowest water depth is reached where $A_0 = 0$. Thus, the model calculations can be considered to be 1.5-D as the horizontal two-dimensional morphology of the lake is taken into account.

Finally, the flux of solute a across the SWI leads to a change of the water column concentration, which is estimated at each time step for each layer below the "èediment effective depth":

$$C^a_{i,j+1} = C^a_{i,j} + F^a_j \frac{A_i - A_{i-1}}{V_i} \Delta t, \quad (4)$$

where V_i is the volume of ith layer of water column and Δt is the time step of the coupled model. A mass balance check of the coupled model revealed less than 1% error for a 10-year simulation.

The model's short execution time and its execution as a Matlab function (taking parameter values as input and returning performance metrics as output) make it suitable for sensitivity and uncertainty analyses. It enables users to evaluate if parameter values found after optimization are unique and determine if the parameters agree with field data and process knowledge (Jackson-Blake & Starrfelt, 2015). Low model sensitivity to a given parameter or the response of the parameter value to changes in other parameters may lower confidence in the values emerging from the optimization (Dittrich et al., 2009).

2.2. Study Site

Lake Vansjø (59° 23′N, 10° 50′E) is located in the southeastern part of Norway. Its catchment was formed during the last ice age and consists of an accumulation of unconsolidated glacial debris (coarse moraines). The area surrounding the lake presently comprises mainly forest (78%), agricultural area (15%), and open water (7%; Skarbøvik et al., 2019). Lake Vansjø has a surface area of 36 km^2 and comprises several subbasins, the two largest being Storefjorden (eastern basin, draining a catchment of 244 km^2), and Vanemfjorden (western basin, draining a catchment of 58 km^2). The water column of both basins remains oxygenated throughout the year. In this study, we focus on the deeper Storefjorden basin (max depth 41 m, mean depth 8.7 m, and residence time 10 months), which drains into the Vanemfjorden basin through a shallow channel. The hydraulic residence time for the two basins together is estimated at 13 months.

The lake is an important drinking water source for three surrounding municipalities and is used for fishing and recreation. It has a long history of eutrophication from, at least, the 1970s when the systematic monitoring of the lake began. Total P concentrations in Storefjorden typically vary between 20 and 40 µg-P/L (Skarbøvik et al., 2019), that is, above the threshold of good ecological status set by the European Water Framework Directive. Lake Vansjø has experienced blooms of cyanobacteria causing beach closures (Moe et al., 2016). Measures to reduce inputs of phosphorus have not been met with a proportionate level of success (Skarbøvik et al., 2019).

2.3. Sampling, Analysis, and Data Sources

Historical precipitation, temperature, insolation, and wind records for Lake Vansjø were obtained from daily weather data at the Norwegian Meteorological Institute stations 1,715 (Rygge), 1,750 (Floter), and 378 (Igsi), located between the two lake basins (59° 38′N, 10° 79′E). Future climatic conditions were obtained from an ensemble of models used by the Inter-Sectoral Impact Model Intercomparison Project and downloaded from the Centre for Environmental Data Analysis database (Warszawski et al., 2014). The Institute Pierre Simon Laplace General Circulation Model (Dufresne et al., 2013), Geophysical Fluid Dynamics Laboratory Climate Model (Delworth et al., 2012), and Norwegian Earth System Model (Bentsen et al., 2013) provided air temperature projections for the period from 2018 to 2100. We retrieved the results of two representative concentration pathways (RCP) of radiative forcing, 4.5 and 8.5 W/m^2, for each model. The data were linearly interpolated over Lake Vansjø using the nearest three grid points. For weather projections without climate change, the statistically consistent future weather was generated after Chen et al. (2010).

Catchment hydrology and loads of suspended sediments, particulate P, and dissolved species were compiled previously (Couture et al., 2018), using daily measurements of flow and biweekly measurements of water chemistry over a 30-year period (1 January 1983 to 31 December 2013) measured at the gauging station at Hogfoss (Station 3.22.0.1000.1; Norwegian Water Resources and Energy Directorate). Lake water chemistry and temperature data were provided by the Vansjø-Hobøl monitoring program, conducted by the Norwegian Institute for Bioeconomy Research and by the Norwegian Institute for Water Research (Haande et al., 2016). The measurements include temperature, concentrations of dissolved oxygen (DO), total P (TP), orthophosphate-P (DIP), particulate organic phosphorus (POP), and chlorophyll a (Chl-a). These data are available freely through Norwegian Institute for Water Research's online database (http://www.aquamonitor.no) until 2015 and on the Norwegian national database (https://vannmiljo.miljodirektoratet.no).

An undisturbed sediment core was collected at the deepest point of the Storefjorden basin using a modified Kajak-Brinkhurst gravity-type corer with an inner diameter of 8.3 cm. The core was sectioned at 1-cm intervals from the SWI down to 5 cm, at 2-cm intervals from 5- to 15-cm depth and at 5-cm intervals from 15- to 30-cm depth. Samples were transported at 4 ° C before centrifugation at 500 *g* under nitrogen atmosphere (N_2:H_2 97:3%, O_2 < 1 ppmv). The supernatant, hereafter referred to as the pore water fraction, was filtered through a 0.2-μm pore size polypropylene membrane filter (Whatman).

Phosphorus partitioning within the sediment was evaluated using the five-step sequential extraction scheme from Hieltjes and Lijklema (1980), Paludan and Jensen (1995), and Reitzel et al. (2006), where Steps 1 and 2 were carried out under an N_2 atmosphere. Briefly, samples were treated, at a 1:25 sediment:solution ratio, with (1) deionized water for 16 hr at 40 ° C, (2) bicarbonate buffered dithionite (BD) solution for 1 hr at 40 ° C, (3) 0.1 M NaOH for 16 hr at 40 ° C, (4) 0.5 M HCl for 16 hr at 40 ° C, and (5) ashed for 8 hr at 520 ° C and 1.0 M HCl for 16 hr at 120 ° C. Between steps, the supernatant was recovered and filtered through a 0.2-μm pore size polypropylene membrane filter. The following operationally defined fractions are associated with the corresponding sequential extraction steps: loosely bound-P, Fe-P, Al-P, Ca-P, and unreactive-P. POP is estimated by subtracting the molybdate-reactive phosphorus from total phosphorus measured in the NaOH extract (Ahlgren et al., 2011). All solutions were prepared using analytical grade reagents from Fluka, Sigma-Aldrich, or Merck and prepared with 18-Ohm water (Millipore) deoxygenated by cooling boiled water using a N_2 stream. Total Fe, Al, and Ca concentrations of the pore water samples and extracts were measured by ICP-OES (Thermo Scientific iCAP 6300) after acidification with HNO_3 to pH < 2. Total P and soluble reactive P (SRP) were measured by the molybdenum blue/ascorbic acid method on a LaChat QuickChem 8500 flow injection analyzer system. Matrix-matched standards were used for all calibrations, and NIST-validated multielemental solutions were used as controls.

3. Results and Discussion

3.1. Water Column Temperature and Chemistry

Because of the relatively short hydraulic residence time of the lake, initial conditions in the water column only affect the result during the first 10 years of simulation. In contrast to the water column, the sediment contains slowly reacting solid phases, and the module could not be spinned up with measured data only. Instead, the 1983–1995 cycle was repeated until the sediment column reached steady state, at which point the concentration distributions were saved and used as initial conditions in the further simulations of the historical period (1995–2015), open water scenario (1995–2015), climate warming (1995–2070), external P reduction scenario (1995–2200), and Fe amendment scenario (1995–2070).

Six model parameters were optimized to fit the simulated temperatures to observations in the water column of the lake: the open water diffusion a_k, the ice-covered period diffusion parameter a_k^{ice}, the minimum stability frequency N^2, the light attenuation coefficients (photosynthetically $\hat{\varepsilon}$ and nonphotosynthetically active $\bar{\varepsilon}$), and the win sheltering coefficient W_{str} (Table S2). These parameters were taken from previous modeling studies on Lake Vansjø (Couture et al., 2014; Saloranta & Andersen, 2007).

Figure 3 highlights the good agreement between simulated and observed temperatures. The mean absolute error for all depths was 1.07 ° C, RMSE was 1.34 ° C, the correlation coefficient (r) was 0.91, the coefficient of determination (R^2) was 0.7, and the bias was −0.6 ° C (Table S3). In general, the model tended to slightly underestimate the warming of the hypolimnion during summer periods.

Of the 43 parameters values needed for the reaction network, 30 were taken from the literature (Atkin & Tjoelker, 2003; Canavan et al., 2006; Couture et al., 2016; Dijkstra et al., 2018; Katsev & Dittrich, 2013; Parkhurst & Appelo, 2013; Van Cappellen & Wang, 1996), and 13 were fitted to reproduce the observations. The calibrated parameters relate to organic matter degradation, the half-saturation constants of microbial Fe reduction, and P sorption and mineral precipitation parameters. The values remained within the range of previously reported values, as shown in the supporting information (Table S4).

The dissolved oxygen (DO) concentration in the water column declined throughout annual periods of high productivity, reaching minimum values in the hypolimnion at about 0.1 mmol/L (Figure 4). The measurements are more scattered before the year 2010 than afterward, likely reflecting the improved DO measurement protocols introduced in 2010. As can be seen in Figure 4, the model was able to reproduce the observed DO concentration time series in the water column with a bias of less than 9% for the DO concentrations in the hypolimnion. The RMSE gradually increased with the depth, from 0.03 mmol/L at the surface

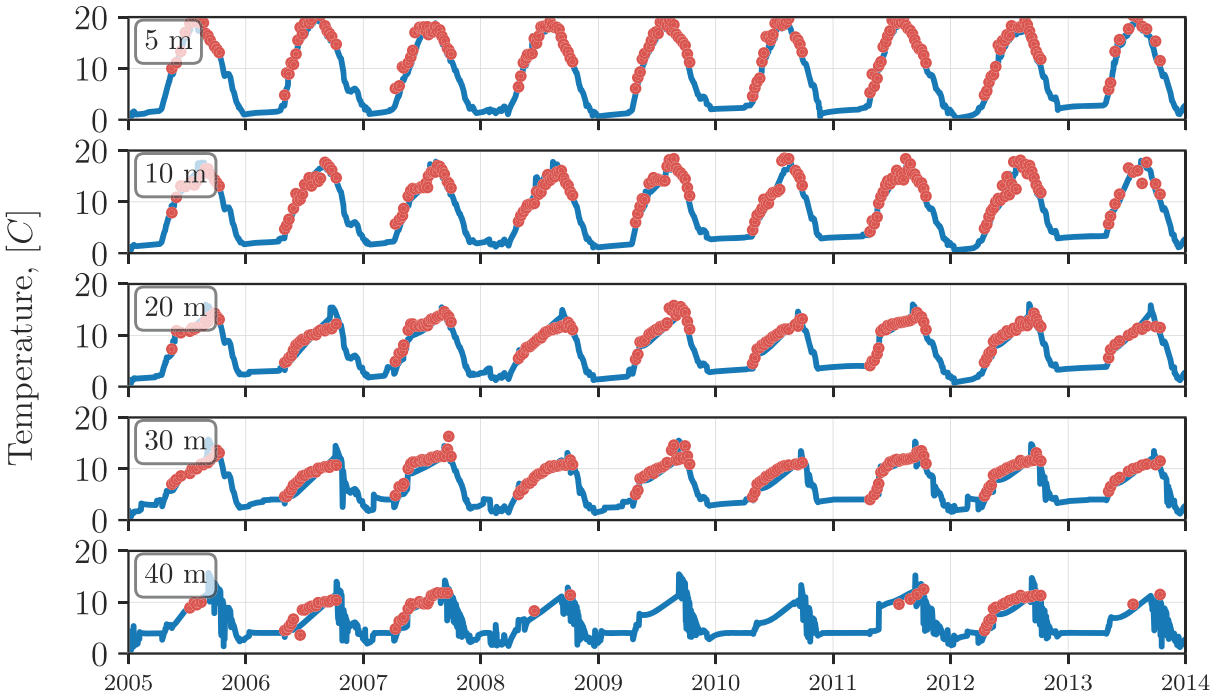

Figure 3. Observed temperatures (symbols) at different depths in Lake Vansjø compared to simulations (lines) with the calibrated physical model for the period from 2005 to 2014.

to 0.1 mmol/L at 40 m (Table S3). Although the timing and magnitude of the DO peaks are well captured, in the specific case of DO at 40-m depth, the model struggles to fully capture the trends, which results in the low statistical correlation metrics (Table S3). The model satisfactorily captured the seasonal variations of total phosphorus (TP), phytoplankton (Phy-P), DIP, and particulate phosphorus (PP) in the mixed layer of the lake (Figure 5). The simulated P dynamics in the lake reproduced the observed strong seasonal features,

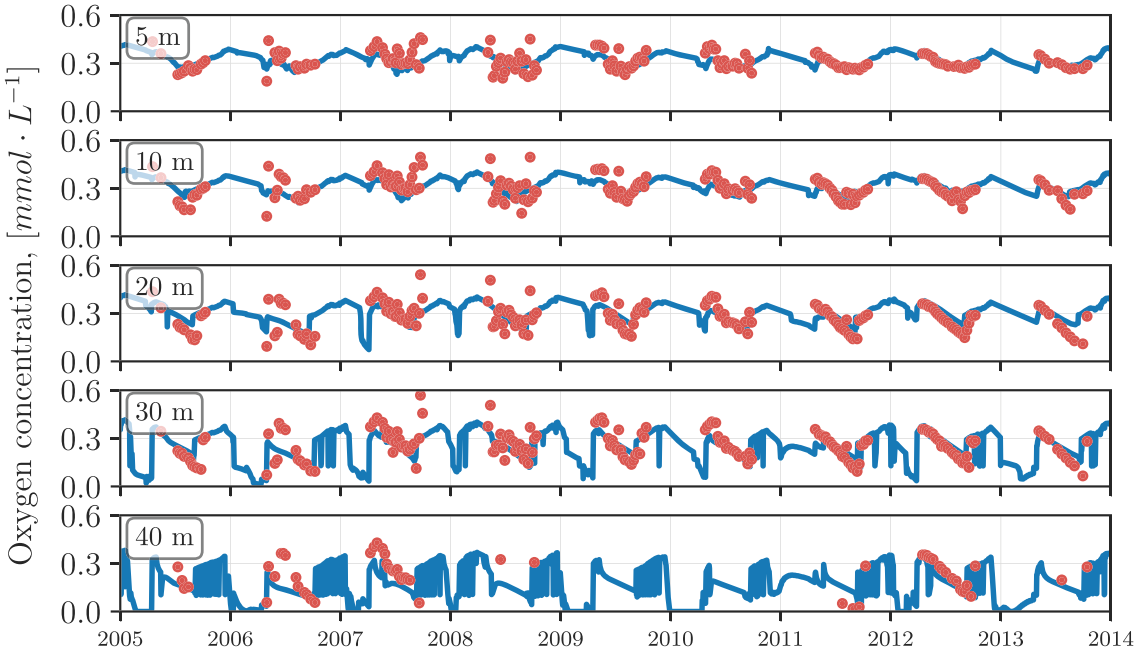

Figure 4. Observed dissolved oxygen concentrations (symbols) at different depths in Lake Vansjø compared to simulations (lines) of the calibrated model for the period from 2005 to 2014.

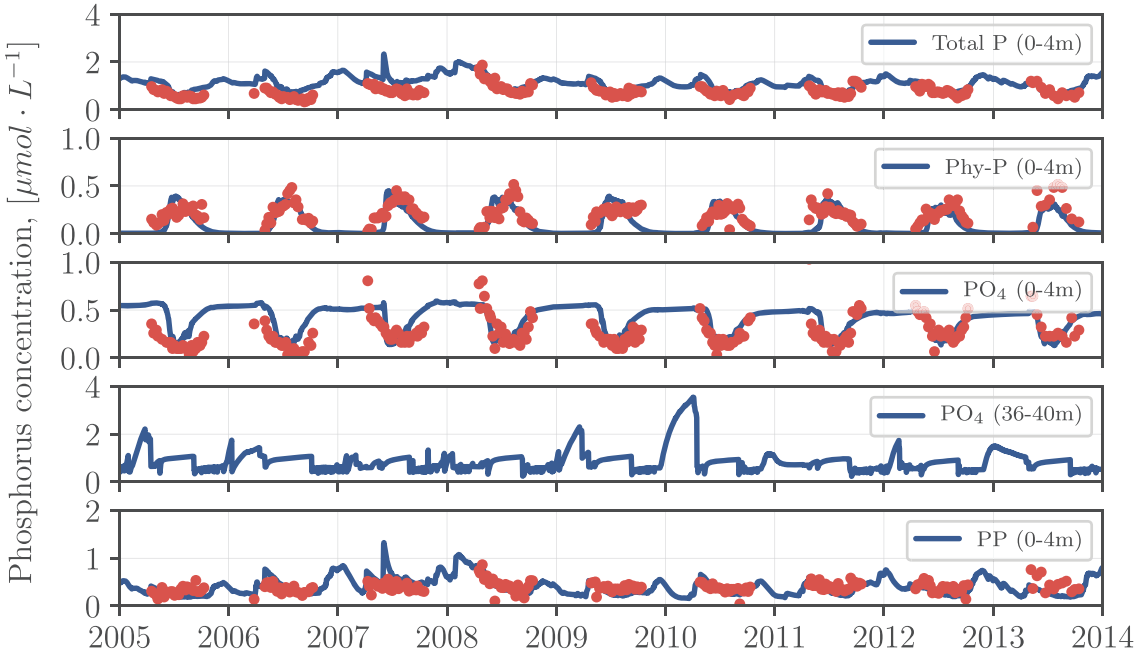

Figure 5. Observed concentrations (symbols) of total phosphorus (Total P) in surface water (0–4 m), phosphorus in phytoplankton (Phy-P) in surface water (0–4 m), dissolved inorganic phosphorus (DIP) in surface and bottom water (36–40 m), and particulate phosphorus (PP) in surface water (0–4 m) compared to simulations (lines) of the calibrated model for the period from 2005 to 2014. Total P is the sum of all phosphorus compounds, i.e., Phy-P, DIP, and particulate organic and inorganic P. Measured Phy-P concentrations are derived from Chl-a measurements using C:Chl-a=40:1 (g/g) and C:P=106:1(mol/mol) ratios (Cloern et al., 1995). PP is the sum of allochthonous particulate organic phosphorus and solid inorganic phosphorus.

with Phy-P reaching maximum values during the summer when the lake is most productive. By contrast, surface DIP is at a minimum during the summer, consistent with its uptake by phytoplankton. Discrepancies between measured and model P distributions in the water column may be due to the simplicity of the algal dynamics in MyLake. Although this version of MyLake adds NO_3^- and NH_4^+ as state variables, it does not yet simulate N-limitation to algal growth or phytoplankton community dynamics, as is done in other models such as PROTECH (Reynolds et al., 2001); thus, community shifts due N recycling from the sediments, or to changing climate, are not captured. Other processes, such as cell buoyancy effects (Gemmell et al., 1840) and grazing by zooplankton (George & Reynolds, 1997), are also not included.

3.2. Sediment Pore Water and Solid-Phase Geochemistry

In the sediment, the pore water concentration of DIP gradually increased with depth from near 0 mM at SWI to about 0.06 mM at 16 cm, then steadily decreased to 0.04 mM at 30 cm (Figure 6.1). In the upper 10 cm, the concentrations of dissolved Fe and Ca increased steadily with depth to their highest values of 0.5 and 0.27 mM, respectively, remaining fairly constant at greater depths. The model captured the main features of the pore water profiles, both the depth of the phosphate and Ca peaks and the magnitudes of the concentrations. The total solid fraction of P in the sediment was about 0.7 mmol/g of dry sediment (2% by weight). Solid-phase P speciation was dominated by Fe-bound phosphorus (Fe-P), followed by Al-bound (Al-P), POP, and Ca-bound phosphorus (Ca-P). In the model, Fe-P is represented by P sorbed on Fe minerals and vivianite, Al-P by P sorbed on Al, POP by allochthonous particulate P, and Phy-P, and Ca-P by apatite. By adjusting the parameters of first-order rate constants of organic matter degradation, dissolution and precipitation constants of vivianite and apatite, and phosphate adsorption constants on Fe and Al oxides, the model also captured the distribution of P in the operationally defined pools (Figure 6.2). The modeling results indicate that the most significant parameters, with respect to P release from the sediment to the water column, are the parameters values describing organic matter lability (first-order rate constants of organic matter degradation), the reductive dissolution of Fe (oxy)hydroxides (half-saturation constants of the terminal electron acceptors), and the sorption of P onto Fe and Al oxides (Table S4). The model-predicted sediment burial rate of 0.1 cm/year falls within the range of 0.07–0.21 cm/year obtained from ^{210}Pb dating of two cores taken in 2005 (Solheim et al., 2006). Thus, the burial rate suggests that the top 15 cm of the sediment represent about 100–150 years of sediment deposition. Finally, although the pore water DO was not measured in

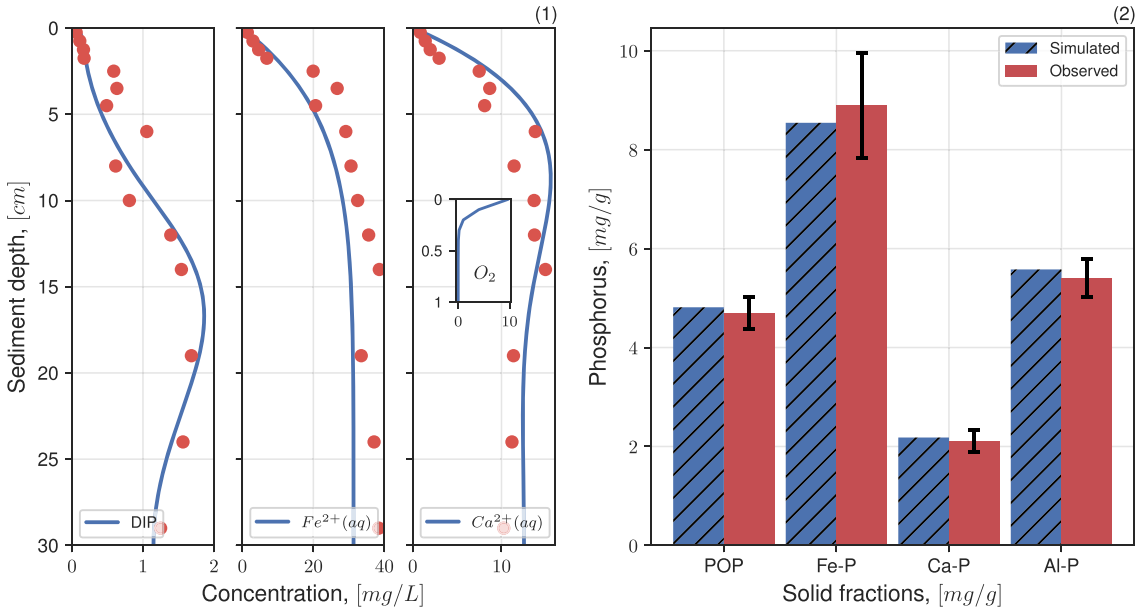

Figure 6. Sediment geochemistry: (1) observed (circles) and simulated (lines) pore water profiles of DIP, ferrous iron, and calcium, along with simulated pore water profile of dissolved oxygen (insert) and (2) observed (solid red) and simulated (blue with diagonal lines) average concentrations of the solid-phase pools of phosphorus in depth interval 0–30 cm. The pore water and solid-phase data were measured on sediment cores collected in October 2014 in the deepest part of Lake Vansjø.

the sediment cores, modeling results predict that it was depleted within the uppermost 0.3 cm of sediment (Figure 6.1, insert). Such DO penetration depth is consistent with high rates of organic matter degradation following the season of high biological productivity (Maerki et al., 2009).

3.3. Baseline Simulation

Depth-integrated P reaction rates, fluxes, and inventories are shown in Figure 7. The simulation results for the historical 1995–2015 period, hereafter referred to as the baseline, indicate that about one third of P deposited at the SWI is sorbed to ferric Fe (oxy)hydroxides and the remaining consists of POP. Upon reductive dissolution of the Fe oxides and microbial degradation of POP, on average 60% of the deposited P is returned as DIP to the overlying water, while 40% remains trapped in the iron redox cycle or precipitates as apatite. Below the upper (0–15 cm) sediment interval of P recycling associated with the reductive dissolution and oxidative precipitation of ferric Fe (oxy)hydroxides, P is permanently removed via the burial of Fe and Ca phosphate mineral phases and P sorbed to Al oxides. Over the historical period, the bottom sediments act as a net sink for P. The P exchanges between the sediments and the overlying water vary significantly along a single year, however. In particular, the sediments become a more pronounced source of P to the water column during the growing season (Figure 8). In the following sections, the baseline serves as the starting point of additional simulations in which various perturbations are imposed on the lake-sediment system, namely, (1) projected future changes in air temperature, (2) disappearing ice-cover, (3) stoppage of external P input, and (4) Fe amendments as a remediation strategy.

3.4. Climate Warming Scenarios

Lakes are warming under climate change worldwide (Woolway & Merchant, 2019). Surface temperatures in seasonally ice-covered lakes have been reported to increase faster than in ice-free lakes (O'Reilly et al., 2015; Winslow et al., 2018). At the same time, significant decreases in the duration of ice cover have been observed and are projected to continue (Austin & Colman, 2008; Butcher et al., 2015; Fang & Stefan, 2009), with profound impacts on water-column processes, as summarized in Lindenschmidt et al. (2018). Lake water quality and harmful algal blooms are expected to worsen as a result of higher water temperatures (Mantzouki et al., 2018), droughts, and longer hydraulic residence times (Mosley, 2015; Visser et al., 2016).

Here we analyze how Lake Vansjø may respond to changing air temperatures and, in particular, how this may affect P exchanges between the bottom sediments and the water column. Historical air temperatures for the period 1995–2015 and those from the climate models described in section 2.3 for the period from 2015

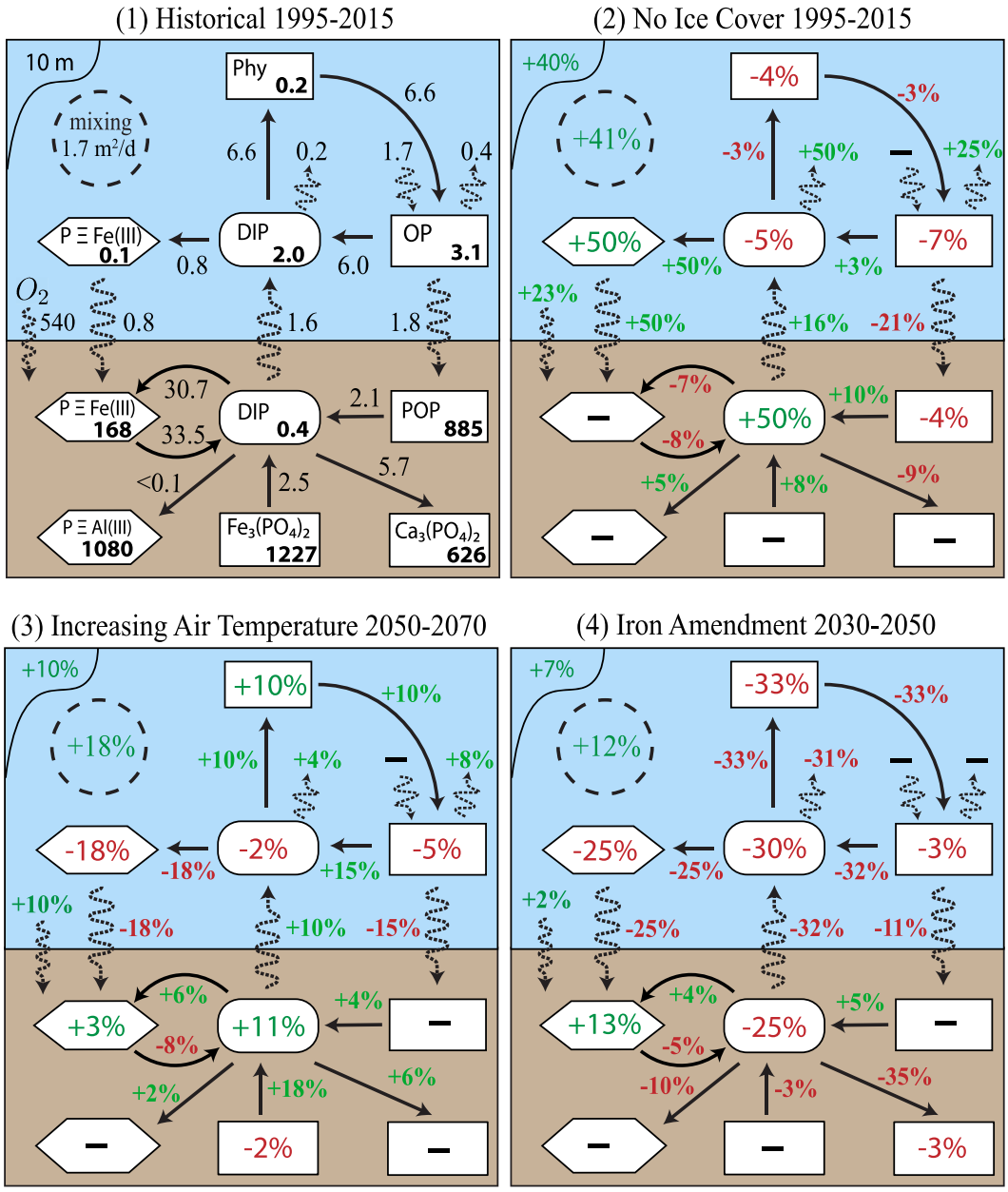

Figure 7. Calculated 20-year average values of P fluxes (μmol-P·cm^{-2}·year^{-1}) and depth-integrated P inventories (μmol-P/cm^{2}) in the water-column and sediment: (1) historical 1995–2015 simulation, (2) no ice cover 1995–2015, (3) increasing air temperatures 2050–2070, and (4) Fe amendment scenario 2030–2050. IPSL, GFDL, and NorESM climate models provided the atmospheric forcing for Scenarios 3 and 4. Dashed zigzag lines represent fluxes in and out of the water column due to lake inflows and outflows as well as transfers across the SWI. Red and green colors represent relative change in values compared to the historical 1995–2015 simulated values. Percentage change within 1% of the original values are noted with dash (no change). OP stands for the sum of particulate and dissolved organic P.

to 2070 were imposed to the model. The largest differences in the projected air temperatures are between the climate models rather than between RCPs: IPSL and GFDL both predict warmer winters (+7 ° C for IPSL and +3 ° C for GFDL) and summers (+3 ° C for IPSL and +0.5 ° C for GFDL), while NorESM predicts warmer winters (+3 ° C) but colder summers (−3 ° C) compared to the historical period (Figure S1). Trends of selected model variables under the climate warming scenarios are summarized in Figure 9 (note that seasonal ice formation is still taking place in the warming scenarios, in contrast to the open water scenario discussed in section 3.5).

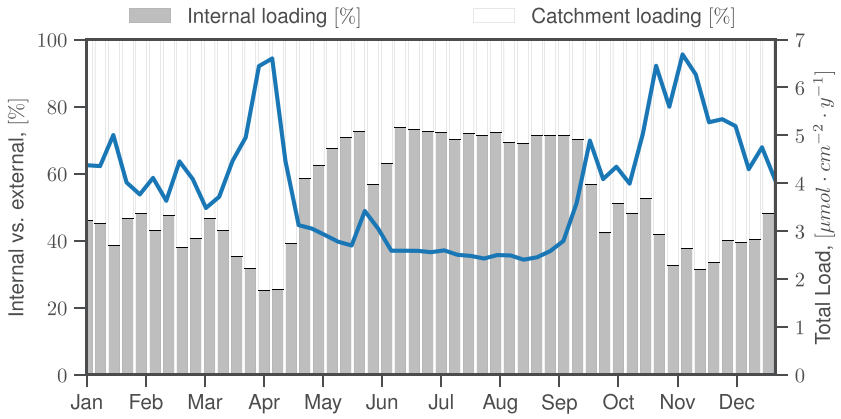

Figure 8. Weekly total P loading (external plus internal) to the water column of Lake Vansjø (blue line), and relative contributions (in %) of P supplied from the catchment (solid white) and from the sediments (solid gray). The results shown are average values for the period 1995–2015.

In agreement with previous studies (Gebre et al., 2014), the model results predict that, on an annual basis, with every degree of air temperature increase, the duration of lake ice shortens by about 21 days (Figure S2). In the "warmest" IPSL RCP 8.5 scenario, the model yields a reduction in ice cover duration from 105 days during the historical period (1995–2015) to less than 20 days for the 2050–2070 period.

Increasing air temperature and decreasing ice cover have antagonistic effects on water column stability. As summarized in Obertegger et al. (2017), decreasing ice cover duration enhances spring mixing as a result of prolonged periods of open water and subsequent wind exposure, an effect that is offset by earlier stratification due to warming air temperatures (Adrian et al., 2009), which in turn slows down DO replenishment of the lower lake waters. Despite an extension of the period of water column stratification by up to 10 days, compared to the historical 1995–2015 period, the cumulative effect of both imposed environmental variations is the gradual deepening of the thermocline, together with increasing vertical mixing (on average) and decreasing duration of hypoxia (Figures 7 and 9). These results are in line with previous studies where shorter ice cover duration is the governing factor driving increasing dissolved oxygen concentrations in the water column (Couture et al., 2015; Fang & Stefan, 2009).

The model results suggest that earlier water column ventilation and late-season warming of the hypolimnion have cascading effects on the biogeochemical dynamics in the sediments. First, increased bottom DO

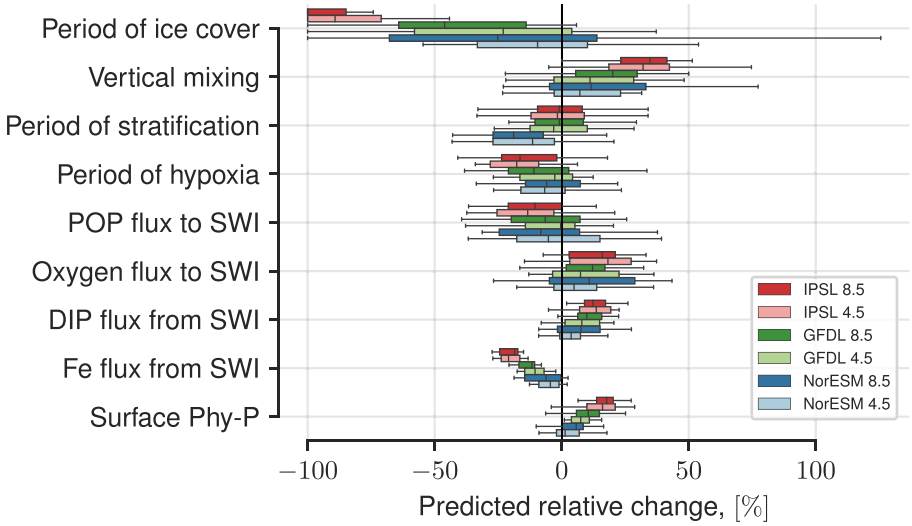

Figure 9. Change of selected MyLake-Sediment output in the climate warming scenarios, according to the projections of the climate models for RCP 4.5 and RCP 8.5 and over the period of 2050–2070, relative to average historical values for the period 1995–2015.

concentration favors both the degradation of organic matter in the sediment and the oxidation of Fe(II). The former releases DIP to the porewater, while the latter forms Fe(III) (oxy)hydroxides that sequester DIP. The model predicts that DIP release exceeds DIP sorption by newly formed Fe (oxy)hydroxides. The net result is a decrease of the Fe(II) and an increase of the DIP flux from the sediment (Figure 9). Next, phytoplankton growth and abundance respond to the increasing internal P loading and the warming water temperature yielding a summer bloom that lasts about 10 days longer by the end of the simulation period (not shown).

3.5. Open Water Scenario

Given the key role of ice cover in controlling water column stability and the biogeochemical dynamics of the lake, we simulate the response to a complete absence of ice cover. This is done by imposing open water conditions throughout the entire simulation period, hence allowing for enhanced gas exchange and wind-induced mixing during the otherwise ice-covered time of the year. The integrated P fluxes and inventories for the open water scenario during the 1995–2015 period, compared to the baseline values, are shown in Figure 7b.

The model results yield averaged vertical diffusivity coefficients that are up to 41% higher without ice than with ice as a result of the enhanced wind-induced mixing. During the course of year, the durations of stratification and hypoxia decrease at first stepwise by about 20% and 50%, respectively (Figure S2), until increasing temperature gradually reverts the trend causing the extension of the period of stratification. As also seen for the shorter ice-covered durations in the climate warming scenarios, the complete absence of ice cover leads to higher dissolved oxygen concentrations in the water column and a 23% rise in the oxygen influx to the sediment. The more oxygenated water column further results in more P to be deposited at the SWI in the form of P sorbed to ferric Fe (oxy)hydroxides, and less as POP. The increased efflux of DIP from the sediments in the year-round open water scenario, however, is mostly supported by the faster early diagenetic mineralization of POP under the more oxic conditions. The enhanced upward vertical mixing of DIP also increases P export via the lake outflow. That is, overall, the lake's sediments become less efficient at retaining P. Nonetheless, despite the profound reorganization of P cycling in the lake, the complete absence of ice cover has only a relatively small impact on the phytoplankton biomass (4% decrease).

3.6. External P Reduction Scenario

To further evaluate the role of internal P loading in the biogeochemical functioning of Lake Vansjø, a simulation is performed where the external loads of all P-containing species are set to zero after 2015, all other conditions remaining unchanged (Figure S3). The simulation is run until 2195, that is, the 20-year historical cycle (1995–2015) is repeated 10 times but without any new addition of P to the lake. Thus, all phytoplankton biomass growth after 2015 is supported by P recycling within the lake-sediment system.

The results indicate that after the external P cutoff internal loading from the sediments provides a long-term source of P to the water column (Figure S3). Prior to the external P cutoff, the efflux of DIP from the sediments represents 25–75% of the total P loading to the water column (Figure 8). After the external P cutoff, it becomes 100% of the total loading. From 2015 onward, the magnitude of the internal DIP loading is predicted to decay exponentially towards a steady-state where the sediment is depleted in reactive P. Such decay can be also simulated with a half-life of 229 years according to the best fit equation: $F_0 \cdot exp(-t/330)$, where F_0 is the DIP efflux before the cutoff and t is the number of years after 2015. The long decay period reflects the slow depletion of the large solid-phase P pools accumulated in the sediment, mainly via DIP production by the degradation of POP, P desorption from Fe, and Al mineral phases and dissolution of vivianite (Figure S3).

The important role of legacy P stored in the sediments is further illustrated by conducting the same simulation but with the sediment module turned off (Figure S3, panel 3). In the absence of internal DIP loading, the lake's temporal response to the external P cutoff is instead driven by the water residence time. The depletion of water column DIP can be approximated by the following fitted curve: $P_0 \cdot exp(-t/3\tau)$, where P_0 is the concentration of DIP before the cutoff and τ is the hydraulic residence time (0.85 years). The Factor 3 in the denominator of the exponent indicates that the decay of the DIP concentration is slower than that expected for an unreactive tracer, because the biological cycling of P in the water column increases the residence time of DIP. That is, nine hydraulic residence times are needed to flush out 95% of DIP. Thus, overall, internal DIP loading extends the response time scale of Lake Vansjø with respect to the cessation of external P loading by more than 2 orders of magnitude relative to the no-sediment scenario.

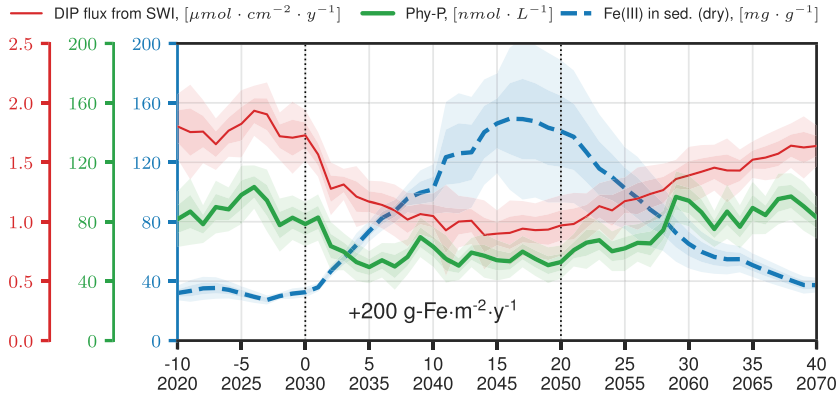

Figure 10. Response of the benthic DIP flux (thin red line), water-column phytoplankton biomass (thick green line), and sediment Fe inventory (dashed blue line) to the addition of 200 g-Fe·m^{-2}·year^{-1}, starting in 2030 and continuing until 2050. The shaded areas represent the ranges obtained for the different air temperature projections from the GFDL, IPSL, and NorESM models shown in Figure S1. Dark- and light-shaded areas represent 68 and 95 confidence intervals, respectively.

Under the current climate conditions, the modeled DIP concentration time series can be used to derive the following predictive model emulator of the average annual DIP concentration in the water column of Lake Vansjø, as a function of the external and internal P loadings:

$$DIP = 3 \cdot \tau \cdot (F_{ext} + F_{sed}) - (3 \cdot \tau \cdot (F_{ext} + F_{sed}) - P_0) \cdot exp(-t/3\tau), \quad (5)$$

where DIP is expressed in units of µmol/L and F_{ext} and F_{sed} are the DIP fluxes to the water column from the catchment and from the sediments, respectively, both expressed in units of µmol·L^{-1}·year^{-1}. This lake-specific equation would predict, for instance, that best management practices that would reduce the external P load by half would decrease the water column DIP concentration by about 20% over a 10-year period.

3.7. Fe Amendment Scenario

While the majority of management measures and practices focus on reducing external P loads to improve water quality in lakes, alternative mitigation approaches rely on the addition of reactive materials to the water column to sequester P in the sediments (Mackay et al., 2014). Because of the strong coupling of the early diagenetic cycling of P and Fe (Molot et al., 2014; Doolittle et al., 2018; Verschoor et al., 2017), materials that have been used include salts of ferric Fe (Engstrom, 2005; Orihel et al., 2016; Wilfert et al., 2015), but also Al (Huser et al., 2016; Schutz et al., 2017) and Ca phases (Gulati et al., 2012), as well as lanthanum clays (Dithmer et al., 2015).

Here, we simulate the outcomes of a ferric Fe addition to Lake Vansjø. The imposed scenario consists of yearly additions, from 2030 to 2050, of 200 g/m^2 (0.3 mmol/cm^2) of Fe(III) added via the lake inlet just before ice breakup. The resulting 20-year averaged fluxes and inventories of the P cycle during the iron treatment are compared to the historical 1995–2015 values in Figure 7, while Figure 10 shows the timing and magnitude of the changes in the DIP efflux from the SWI, phytoplankton biomass, and Fe inventory of the sediments. Figure 11 further shows the relationship between benthic DIP fluxes and annual Fe loads before, during and after Fe treatment. The figure illustrates the hysteresis in the internal DIP loading response after the amendment is terminated in 2050.

During the first 10 years of Fe amendment, the model predicts that the DIP flux from the sediments decreases by 43% from an average annual value of 1.75 to 1 µmol·cm^{-2}·year^{-1} (Figure 10). This decline in internal P loading is due to enhanced P retention in the sediments by Fe(III) (oxy)hydroxide minerals in the upper oxic layer and by ferrous Fe minerals, such as vivianite, in the deeper anoxic layer (Bostrom et al., 1988; Smolders et al., 2006). The decreased internal P loading in turn results in lower phytoplankton biomass, which decreases by 30% from 85 to 60 nmol-P/L during the period of amendment (Figure 10). Once the treatment is terminated (i.e., from 2050 onward), the lake's phytoplankton biomass returns to its pretreatment level within about 15 years (Figure 10). The imposed Fe treatment and the predicted responses are consistent

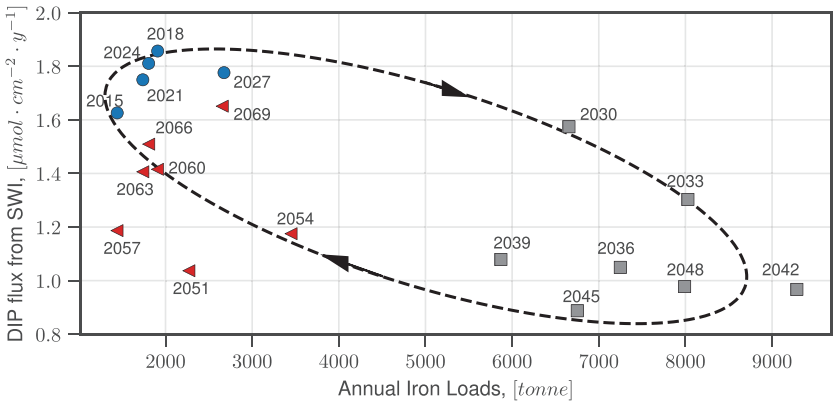

Figure 11. Relationship between the annual benthic flux of DIP from sediment to water column (i.e., the internal P loading) and the corresponding annual ferric Fe loading to the lake before the iron amendment (2015–2030; circles), throughout the amendment period (2030–2050; squares) and after the amendment (2050–2070; triangles). Dashed line and arrows highlight the direction of the hysteresis of the relationship.

with observations reported for 15 actual treatments worldwide (Orihel et al., 2016), in which lakes with low natural Fe levels show stronger responses than Fe-rich lakes.

The efficiency with which Fe amendments are likely to decrease algal growth depends on the existing Fe inventory in the sediments, and on whether or not internal loading is a major source of DIP to the water column. For example, in Lake Simcoe (Ontario, Canada), similar to Lake Vansjø, internal loading supplies between a third to one half of P to the water column (Loh, 2013). In contrast, the estimated internal loading in the eastern basin of Lake Erie (Ontario, Canada) only accounts for 3–7% of the total phosphorus load (Matisoff et al., 2016). In such a case, even if the addition of Fe reduces the internal loading by half, the overall effect will be insignificant.

Finally, internal P loading has been shown to be naturally suppressed in lakes with sediments containing high concentrations of Al (Kopácek et al., 2005; Ostrofsky, 2019; Lake et al., 2007). Additions of Al have been used as a lake remediation measure, and studies of Al-treated lakes show that Al enhances P sorption in sediments and prevent P release to the water column even if the reductive dissolution of Fe(III) minerals occurs (Huser et al., 2016). The use of MyLake-Sediment model to simulate a lake's response to Al addition, however, will require careful modeling of lake and porewater pH in order to capture the pH-dependent P sorption to Al mineral phases (Reitzel et al., 2013).

4. Concluding Remarks

Internal nutrient recycling from sediments plays a key role in the biogeochemical cycling and biological productivity of lakes. Here, we present a Lake-Sediment model meant to diagnose the processes driving internal P loading in lakes and predict how these processes respond to changes in climate conditions, inputs from the catchment, and lake restoration measures. The model directly couples the biogeochemical reaction networks of water column and sediments in order to simulate P exchanges across the SWI. We use the model to assess the effectiveness of P loading targets and other mitigation strategies aimed at controlling excessive algal growth in a eutrophic lake. The results clearly illustrate the importance of the accumulated legacy P in the lake's sediments in controlling the timing and magnitude of the response of internal P loading to external forcings, including projected changes in air temperature and ice cover, as well as management interventions.

With a strong focus on coupled biogeochemical processes across the SWI, this code can serve as a stepping stone to generate lake restoration scenarios (Lürling et al., 2016), test hypotheses on the response of algal biomass to external and internal fluxes of P and Fe (Verschoor et al., 2017), and help with "climate-proofing" remediation measures, whose effectiveness will likely be modulated by ongoing climate change (Trolle et al., 2011). To this end, further model development and evaluation avenues should focus on capturing the temporal (e.g., Amirbahman et al., 2012; Katsev and Dittrich ; 2013) and, in particular, spatial heterogeneity in sediment P distributions and recycling efficiencies (e.g., Dittrich et al., 2013; Doan et al., 2018; Gudimov et al., 2015; Matisoff et al., 2017, 2016).

Acknowledgments
R. M. C. acknowledges funding from the Research Council of Norway (Lakes in Transition, Project 244558), the Canada First Research Excellence Fund Program (Sentinel North Research Chair in Aquatic Geochemistry), and the NSERC Discovery grant program. P. V. C. acknowledges funding from the Canada Excellence Research Chair in Ecohydrology and the Canada First Research Excellence Fund Program (Lake Futures project of Global Water Futures). We thank Marcia Kyle for help in the field as well as Chris Parsons and Marianne Vandergriendt for help in the laboratory. The MyLake-Sediment source code is publicly available on GitHub (at https://github.com/biogeochemistry/MyLake_v2_Vansjo). Input and output data are available in open access (at https://www.frdr.ca/repo/handle/doi:10.20383/101.0149).

References

Adrian, R., O'Reilly, C. M., Zagarese, H., Baines, S. B., Hessen, D. O., Keller, W., et al. (2009). Lakes as sentinels of climate change. *Limnology and Oceanography*, *54*(6), 2283–2297.

Ahlgren, J., Reitzel, K., De Brabandere, H., Gogoll, A., & Rydin, E. (2011). Release of organic P forms from lake sediments. *Water Research*, *45*(2), 565–572. https://doi.org/10.1016/j.watres.2010.09.020

Akbarzadeh, Z., Laverman, A. M., Rezanezhad, F., Raimonet, M., Viollier, E., Shafei, B., & Van Cappellen, P. (2018). Benthic nitrite exchanges in the Seine River (France): An early diagenetic modeling analysis. *The Science of the Total Environment*, *628-629*, 580–593. https://doi.org/10.1016/j.scitotenv.2018.01.319

Amirbahman, A., Lake, B. A., & Norton, S. A. (2012). Seasonal phosphorus dynamics in the surficial sediment of two shallow temperate lakes: A solid-phase and pore-water study. *Hydrobiologia*, *701*(1), 65–77. https://doi.org/10.1007/s10750-012-1257-z

Atkin, O. K., & Tjoelker, M. G. (2003). Thermal acclimation and the dynamic response of plant respiration to temperature. *Trends in Plant Science*, *8*(7), 343–351. https://doi.org/10.1016/S1360-1385(03)00136-5

Austin, J., & Colman, S. (2008). A century of temperature variability in Lake Superior. *Limnology and Oceanography*, *53*(6), 2724–2730. https://doi.org/10.4319/lo.2008.53.6.2724

Bentsen, M., Bethke, I., Debernard, J. B., Iversen, T., Kirkevaag, A., Seland, O., et al. (2013). The Norwegian Earth System Model, NorESM1-M—Part 1: Description and basic evaluation of the physical climate. *Geoscientific Model Development*, *6*(3), 687–720. https://doi.org/10.5194/gmd-6-687-2013

Bostrom, B., Andersen, J. M., Fleischer, S., & Jansson, M. (1988). Exchange of phosphorus across the sediment-water interface. *Hydrobiologia*, *170*(1), 229–244. https://doi.org/10.1007/bf00024907

Boudreau, B. P. (1997). *Diagenetic models and their implementation*. Heidelberg: Springer. https://doi.org/10.1007/978-3-642-60421-8

Bryhn, A. C., & Haakanson, L. (2007). A comparison of predictive phosphorus load-concentration models for lakes. *Ecosystems*, *10*(7), 1084–1099. https://doi.org/10.1007/s10021-007-9078-z

Butcher, J. B., Nover, D., Johnson, T. E., & Clark, C. M. (2015). Sensitivity of lake thermal and mixing dynamics to climate change. *Climatic Change*, *129*(1-2), 295–305. https://doi.org/10.1007/s10584-015-1326-1

Canavan, R. W., Slomp, C. P., Jourabchi, P., Van Cappellen, P., Laverman, A. M., & van den Berg, G. A. (2006). Organic matter mineralization in sediment of a coastal freshwater lake and response to salinization. *Geochimica et Cosmochimica Acta*, *70*(11), 2836–2855. https://doi.org/10.1016/j.gca.2006.03.012

Carvalho, L., McDonald, C., de Hoyos, C., Mischke, U., Phillips, G., Borics, G., et al. (2013). Sustaining recreational quality of European lakes: minimizing the health risks from algal blooms through phosphorus control. *The Journal of Applied Ecology*, *50*(2), 315–323. https://doi.org/10.1111/1365-2664.12059

Chen, J., Brissette, F. P., & Leconte, R. (2010). A daily stochastic weather generator for preserving low-frequency of climate variability. *Journal of Hydrology*, *388*(3-4), 480–490. https://doi.org/10.1016/j.jhydrol.2010.05.032

Cloern, J. E., Grenz, C., & Lucas, L. V. (1995). An empirical model of the phytoplankton chlorophyll: Carbon ratio-the conversion factor between productivity and growth rate. *Limnology and Oceanography*, *40*(7), 1313–1321. https://doi.org/10.4319/lo.1995.40.7.1313

Couture, R.-M., de Wit, H. A., Tominaga, K., Kiuru, P., & Markelov, I. (2015). Oxygen dynamics in a boreal lake responds to long-term changes in climate, ice phenology, and DOC inputs. *Journal of Geophysical Research: Biogeosciences*, *120*, 2441–2456. https://doi.org/10.1002/2015jg003065

Couture, R.-M., Fischer, R., Van Cappellen, P., & Gobeil, C. (2016). Non-steady state diagenesis of organic and inorganic sulfur in lake sediments. *Geochimica et Cosmochimica Acta*, *194*, 15–33. https://doi.org/10.1016/j.gca.2016.08.029

Couture, R.-M., Gobeil, C., & Tessier, A. (2010). Arsenic, iron and sulfur co-diagenesis in lake sediments. *Geochimica et Cosmochimica Acta*, *74*(4), 1238–1255. https://doi.org/10.1016/j.gca.2009.11.028

Couture, R.-M., Jannicke Moe, S., Lin, Y., Kaste, O., Haande, S., & Solheim, A. L. (2018). Simulating water quality and ecological status of Lake Vansjo, Norway, under land-use and climate change by linking process-oriented models with a Bayesian network. *The Science of the Total Environment*, *621*, 713–724. https://doi.org/10.1016/j.scitotenv.2017.11.303

Couture, R.-M., Shafei, B., Van Cappellen, P., Tessier, A., & Gobeil, C. (2010). Non-steady state modeling of arsenic diagenesis in lake sediments. *Environmental Science & Technology*, *44*(1), 197–203. https://doi.org/10.1021/es902077q

Couture, R.-M., Tominaga, K., Starrfelt, J., Jannicke Moe, S., Kaste, O., & Wright, R. F. (2014). Modelling phosphorus loading and algal blooms in a Nordic agricultural catchment-lake system under changing land-use and climate, Environmental Science. *Processes & Impacts*, *16*(7), 1588–1599. https://doi.org/10.1039/c3em00630a

de Wit, H. A., Couture, R.-M., Jackson-Blake, L., Futter, M. N., Valinia, S., Austnes, K., et al. (2018). Pipes or chimneys? For carbon cycling in small boreal lakes, precipitation matters most. *Limnology and Oceanography Letters*, *3*(3), 275–284. https://doi.org/10.1002/lol2.10077

Delworth, T. L., Rosati, A., Anderson, W., Adcroft, A. J., Balaji, V., Benson, R., et al. (2012). Simulated climate and climate change in the GFDL CM2.5 high-resolution coupled climate model. *Journal of Climate*, *25*(8), 2755–2781. https://doi.org/10.1175/jcli-d-11-00316.1

Dibike, Y., Prowse, T., Saloranta, T., & Ahmed, R. (2011). Response of Northern Hemisphere lake-ice cover and lake-water thermal structure patterns to a changing climate. *Hydrological Processes*, *25*, 2942–2953. https://doi.org/10.1002/hyp.8068

Dijkstra, N., Hagens, M., Egger, M., & Slomp, C. P. (2018). Post-depositional formation of vivianite-type minerals alters sediment phosphorus records. *Biogeosciences*, *15*(3), 861–883. https://doi.org/10.5194/bg-15-861-2018

Dithmer, L., Lipton, A. S., Reitzel, K., Warner, T. E., Lundberg, D., & Nielsen, U. G. (2015). Characterization of phosphate sequestration by a lanthanum modified bentonite clay: A solid-state NMR, EXAFS, and PXRD study. *Environmental Science & Technology*, *49*(7), 4559–4566. https://doi.org/10.1021/es506182s

Dittrich, M., Chesnyuk, A., Gudimov, A., McCulloch, J., Quazi, S., Young, J., et al. (2013). Phosphorus retention in a mesotrophic lake under transient loading conditions: Insights from a sediment phosphorus binding form study. *Water Research*, *47*(3), 1433–1447. https://doi.org/10.1016/j.watres.2012.12.006

Dittrich, M., Wehrli, B., & Reichert, P. (2009). Lake sediments during the transient eutrophication period: Reactive-transport model and identifiability study. *Ecological Modelling*, *220*(20), 2751–2769. https://doi.org/10.1016/j.ecolmodel.2009.07.015

Doan, P. T. K., Watson, S. B., Markovic, S., Liang, A., Guo, J., Mugalingam, S., et al. (2018). Phosphorus retention and internal loading in the Bay of Quinte, Lake Ontario, using diagenetic modelling. *Science of The Total Environment*, *636*, 39–51. https://doi.org/10.1016/j.scitotenv.2018.04.252

Doolittle, H. A., Norton, S. A., Bacon, L. C., Ewing, H. A., & Amirbahman, A. (2018). The internal and watershed controls on hypolimnetic sediment phosphorus release in Lake Auburn, Maine, USA. *Lake and Reservoir Management*, *34*(3), 258–269. https://doi.org/10.1080/10402381.2018.1423588

Dufresne, J.-L., Foujols, M.-A., Denvil, S., Caubel, A., Marti, O., Aumont, O., et al. (2013). Climate change projections using the IPSL-CM5 Earth System Model: From CMIP3 to CMIP5. *Climate Dynamics*, *40*(9-10), 2123–2165. https://doi.org/10.1007/s00382-012-1636-1

Engstrom, D. R. (2005). Long-term changes in iron and phosphorus sedimentation in Vadnais Lake, Minnesota, resulting from ferric chloride addition and hypolimnetic aeration. *Lake and Reservoir Management*, *21*(1), 95–105. https://doi.org/10.1080/07438140509354417

Fang, X., & Stefan, H. G. (2009). Simulations of climate effects on water temperature, dissolved oxygen, and ice and snow covers in lakes of the contiguous U.S. under past and future climate scenarios. *Limnology and Oceanography*, *54*(6part2), 2359–2370. https://doi.org/10.4319/lo.2009.54.6_part_2.2359

Franz, D., Mammarella, I., Boike, J., Kirillin, G., Vesala, T., Bornemann, N., et al. (2018). Lake-atmosphere heat flux dynamics of a thermokarst lake in arctic Siberia. *Journal of Geophysical Research: Atmospheres*, *123*, 5222–5239. https://doi.org/10.1029/2017jd027751

Gebre, S., Boissy, T., & Alfredsen, K. (2014). Sensitivity of lake ice regimes to climate change in the Nordic region. *The Cryosphere*, *8*(4), 1589–1605. https://doi.org/10.5194/tc-8-1589-2014

Gemmell, B. J., Oh, G., Buskey, E. J., & Villareal, T. A. (1840). (2016), Dynamic sinking behaviour in marine phytoplankton: Rapid changes in buoyancy may aid in nutrient uptake. *Proceedings of the Royal Society B: Biological Sciences*, *283*(20161), 126. https://doi.org/10.1098/rspb.2016.1126

George, D. G., & Reynolds, C. S. (1997). Zooplankton-phytoplankton interactions: The case for refining methods, measurements and models. *Aquatic Ecology*, *31*(1), 59–71. https://doi.org/10.1023/A:1009920214357

Gudimov, A., Kim, D.-k., Young, J. D., Palmer, M. E., Dittrich, M., Winter, J. G., et al. (2015). Examination of the role of dreissenids and macrophytes in the phosphorus dynamics of Lake Simcoe, Ontario, Canada. *Ecological Informatics*, *26*, 36–53. https://doi.org/10.1016/j.ecoinf.2014.11.007

Gudimov, A., McCulloch, J., Chen, J., Doan, P., Arhonditsis, G., & Dittrich, M. (2016). Modeling the interplay between deepwater oxygen dynamics and sediment diagenesis in a hard-water mesotrophic lake. *Ecological Informatics*, *31*, 59–69. https://doi.org/10.1016/j.ecoinf.2015.11.005

Gulati, R. D., Miguel Dionisio Pires, L., & van Donk, E. (2012). Restoration of freshwater lakes, *Restoration Ecology* (pp. 233–247). Chichester, UK: Wiley-Blackwell: https://doi.org/10.1002/9781118223130.ch18

Haande, S., Jannicke Moe, S., & Couture, R.-M. (2016). Phytoplankton and other monitoring data from Lake VansjO. *Freshwater Metadata Journal*, *15*, 1–8. https://doi.org/10.15504/fmj.2016.15

Hadley, K. R., Paterson, A. M., Hall, R. I., & Smol, J. P. (2012). Effects of multiple stressors on lakes in south-central Ontario: 15 years of change in lakewater chemistry and sedimentary diatom assemblages. *Aquatic Sciences*, *75*(3), 349–360. https://doi.org/10.1007/s00027-012-0280-5

Hieltjes, A. H. M., & Lijklema, L. (1980). Fractionation of inorganic phosphates in calcareous sediments 1. *Journal of Environmental Quality*, *9*(3), 405. https://doi.org/10.2134/jeq1980.00472425000900030015x

Hipsey, M. R., Bruce, L. C., Boon, C., Busch, B., Carey, C. C., Hamilton, D. P., et al. (2017). A General Lake Model (GLM 2.4) for linking with high-frequency sensor data from the Global Lake Ecological Observatory Network (GLEON). *Geoscientific Model Development Discussions*, *12*, 1–60. https://doi.org/10.5194/gmd-2017-257

Hu, F., Bolding, K., Bruggeman, J., Jeppesen, E., Flindt, M. R., van Gerven, L., et al. (2016). FABM-PCLake—Linking aquatic ecology with hydrodynamics. *Geoscientific Model Development*, *9*(6), 2271–2278. https://doi.org/10.5194/gmd-9-2271-2016

Huser, B. J., Egemose, S., Harper, H., Hupfer, M., Jensen, H., Pilgrim, K. M., et al. (2016). Longevity and effectiveness of aluminum addition to reduce sediment phosphorus release and restore lake water quality. *Water research*, *97*, 122–132. https://doi.org/10.1016/j.watres.2015.06.051

Iho, A., Ahlvik, L., Ekholm, P., Lehtoranta, J., & Kortelainen, P. (2017). Optimal phosphorus abatement redefined: Insights from coupled element cycles. *Ecological Economics*, *137*, 13–19. https://doi.org/10.1016/j.ecolecon.2017.02.023

Jackson-Blake, L. A., & Starrfelt, J. (2015). Do higher data frequency and Bayesian auto-calibration lead to better model calibration? Insights from an application of INCA-P, a process-based river phosphorus model. *Journal of Hydrology*, *527*, 641–655. https://doi.org/10.1016/j.jhydrol.2015.05.001

James, W. F. (2017). Internal phosphorus loading contributions from deposited and resuspended sediment to the Lake of the Woods. *Lake and Reservoir Management*, *33*(4), 347–359. https://doi.org/10.1080/10402381.2017.1312647

Janssen, A. B. G., Arhonditsis, G. B., Beusen, A., Bolding, K., Bruce, L., Bruggeman, J., et al. (2015). Exploring, exploiting and evolving diversity of aquatic ecosystem models: a community perspective. *Aquatic Ecology*, *49*(4), 513–548. https://doi.org/10.1007/s10452-015-9544-1

Katsev, S. (2017). When large lakes respond fast: A parsimonious model for phosphorus dynamics. *Journal of Great Lakes Research*, *43*(1), 199–204. https://doi.org/10.1016/j.jglr.2016.10.012

Katsev, S., & Dittrich, M. (2013). Modeling of decadal scale phosphorus retention in lake sediment under varying redox conditions. *Ecological Modelling*, *251*, 246–259. https://doi.org/10.1016/j.ecolmodel.2012.12.008

Katsev, S., Tsandev, I., L'Heureux, I., & Rancourt, D. G. (2006). Factors controlling long-term phosphorus efflux from lake sediments: Exploratory reactive-transport modeling. *Chemical Geology*, *234*(1-2), 127–147. https://doi.org/10.1016/j.chemgeo.2006.05.001

Kiuru, P., Ojala, A., Mammarella, I., Heiskanen, J., Kämäräinen, M., Vesala, T., & Huttula, T. (2018). Effects of climate change on CO2 concentration and efflux in a humic boreal lake: A modeling study. *Journal of Geophysical Research: Biogeosciences*, *123*, 2212–2233. https://doi.org/10.1029/2018JG004585

Kopácek, J., Borovec, J., Hejzlar, J., Ulrich, K.-U., Norton, S. A., & Amirbahman, A. (2005). Aluminum control of phosphorus sorption by lake sediments. *Environmental Science &, Technology*, *39*(22), 8784–8789. https://doi.org/10.1021/es050916b

Lake, B. A., Coolidge, K. M., Norton, S. A., & Amirbahman, A. (2007). Factors contributing to the internal loading of phosphorus from anoxic sediments in six Maine, USA, lakes. *Science of The Total Environment*, *373*(2-3), 534–541. https://doi.org/10.1016/j.scitotenv.2006.12.021

Lehtoranta, J., Ekholm, P., & Pitkanen, H. (2009). Coastal eutrophication thresholds: A matter of sediment microbial processes. *AMBIO: A Journal of the Human Environment*, *38*(6), 303–308. https://doi.org/10.1579/09-a-656.1

Li, J., Zhang, Y., & Katsev, S. (2018). Phosphorus recycling in deeply oxygenated sediments in Lake Superior controlled by organic matter mineralization. *Limnology and Oceanography*, *63*, 1372–1385. https://doi.org/10.1002/lno.10778

Lindenschmidt, K.-E., Baulch, H. M., & Cavaliere, E. (2018). River and lake ice processes—Impacts of freshwater ice on aquatic ecosystems in a changing globe. *Water*, *10*(11), 1586. https://doi.org/10.3390/w10111586

Livingstone, D. M. (2008). A change of climate provokes a change of paradigm: Taking leave of two tacit assumptions about physical lake forcing. *International Review of Hydrobiology*, *93*(4-5), 404–414. https://doi.org/10.1002/iroh.200811061

Loh, P. (2013). Evaluating relationships between sediment chemistry and anoxic phosphorus and iron release across three different water bodies. *Inland Waters*, *3*(1), 105–118. https://doi.org/10.5268/iw-3.1.533

Ludsin, S. A., Kershner, M. W., Blocksom, K. A., Knight, R. L., & Stein, R. A. (2001). Life after death in Lake Erie: Nutrient controls drive fish species richness, rehabilitation. *Ecological Applications: a Publication of the Ecological Society of America*, *11*(3), 731. https://doi.org/10.2307/3061113

Lürling, M., Mackay, E., Reitzel, K., & Spears, B. M. (2016). Editorial—A critical perspective on geo-engineering for eutrophication management in lakes. *Water research*, *97*, 1–10. https://doi.org/10.1016/j.watres.2016.03.035

Mackay, E., Maberly, S., Pan, G., Reitzel, K., Bruere, A., Corker, N., et al. (2014). Geoengineering in lakes: Welcome attraction or fatal distraction? *Inland Waters*, *4*(4), 349–356. https://doi.org/10.5268/iw-4.4.769

Maerki, M., Müller, B., Dinkel, C., & Wehrli, B. (2009). Mineralization pathways in lake sediments with different oxygen and organic carbon supply. *Limnology and Oceanography*, *54*(2), 428–438. https://doi.org/10.2307/40271695

Magnuson, J. J., Robertson, D. M., Benson, B. J., Wynne, R. H., Livingstone, D. M., Arai, T., et al. (2000). Historical trends in lake and river ice cover in the Northern Hemisphere. *Science*, *289*(5485), 1743–1746.

Mantzouki, E., Lürling, M., Fastner, J., de Senerpont Domis, L., & Wilk-Wo Zniak, E. (2018). Temperature effects explain continental scale distribution of cyanobacterial toxins. *Toxins*, *10*(4), 156. https://doi.org/10.3390/toxins10040156

Matisoff, G., Kaltenberg, E. M., Steely, R. L., Hummel, S. K., Seo, J., Gibbons, K. J., et al. (2016). Internal loading of phosphorus in western Lake Erie. *Journal of Great Lakes Research*, *42*(4), 775–788. https://doi.org/10.1016/j.jglr.2016.04.004

Matisoff, G., Watson, S. B., Guo, J., Duewiger, A., & Steely, R. (2017). Sediment and nutrient distribution and resuspension in Lake Winnipeg. *Science of The Total Environment*, *575*, 173–186. https://doi.org/10.1016/j.scitotenv.2016.09.227

Matzinger, A., Muller, B., Niederhauser, P., Schmid, M., & Wuest, A. (2010). Hypolimnetic oxygen consumption by sediment-based reduced substances in former eutrophic lakes. *Limnology and Oceanography*, *55*(5), 2073–2084. https://doi.org/10.4319/lo.2010.55.5.2073

McCulloch, J., Gudimov, A., Arhonditsis, G., Chesnyuk, A., & Dittrich, M. (2013). Dynamics of P-binding forms in sediments of a mesotrophic hard-water lake: Insights from non-steady state reactive-transport modeling, sensitivity and identifiability analysis. *Chemical Geology*, *354*, 216–232. https://doi.org/10.1016/j.chemgeo.2013.06.011

Moe, S. J., Jannicke Moe, S., Haande, S., & Couture, R.-M. (2016). Climate change, cyanobacteria blooms and ecological status of lakes: A Bayesian network approach. *Ecological Modelling*, *337*, 330–347. https://doi.org/10.1016/j.ecolmodel.2016.07.004

Molot, L. A., Watson, S. B., Creed, I. F., Trick, C. G., McCabe, S. K., Verschoor, M. J., et al. (2014). A novel model for cyanobacteria bloom formation: the critical role of anoxia and ferrous iron. *Freshwater Biology*, *59*(6), 1323–1340. https://doi.org/10.1111/fwb.12334

Mooij, W. M., Trolle, D., Jeppesen, E., Arhonditsis, G., Belolipetsky, P. V., Chitamwebwa, D. B. R., et al. (2011). Challenges and opportunities for integrating lake ecosystem modelling approaches. *Aquatic Ecology*, *44*, 633–667.

Mosley, L. M. (2015). Drought impacts on the water quality of freshwater systems; review and integration. *Earth-Science Reviews*, *140*, 203–214. https://doi.org/10.1016/j.earscirev.2014.11.010

Mueller, H., Hamilton, D. P., & Doole, G. J. (2016). Evaluating services and damage costs of degradation of a major lake ecosystem. *Ecosystem Services*, *22*, 370–380. https://doi.org/10.1016/j.ecoser.2016.02.037

Nurnberg, G. K., LaZerte, B. D., Loh, P. S., & Molot, L. A. (2013). Quantification of internal phosphorus load in large, partially polymictic and mesotrophic Lake Simcoe, Ontario. *Journal of Great Lakes Research*, *39*(2), 271–279. https://doi.org/10.1016/j.jglr.2013.03.017

O'Reilly, C. M., Sharma, S., Gray, D. K., Hampton, S. E., Read, J. S., Rowley, R. J., et al. (2015). Rapid and highly variable warming of lake surface waters around the globe. *Geophysical Research Letters*, *42*, 10,773–10,781. https://doi.org/10.1002/2015GL066235

Obertegger, U., Obrador, B., & Flaim, G. (2017). Dissolved oxygen dynamics under ice: Three winters of high-frequency data from Lake Tovel, Italy. *Water Resources Research*, *53*, 7234–7246. https://doi.org/10.1002/2017WR020599

Orihel, D. M., Baulch, H. M., Casson, N. J., North, R. L., Parsons, C. T., Seckar, D. C. M., & Venkiteswaran, J. J. (2017). Internal phosphorus loading in Canadian fresh waters: A critical review and data analysis. *Canadian Journal of Fisheries and Aquatic Sciences*, *74*(12), 2005–2029. https://doi.org/10.1139/cjfas-2016-0500

Orihel, D. M., Schindler, D. W., Ballard, N. C., Wilson, L. R., & Vinebrooke, R. D. (2016). Experimental iron amendment suppresses toxic cyanobacteria in a hypereutrophic lake. *Ecological applications: a publication of the Ecological Society of America*, *26*(5), 1517–1534. https://doi.org/10.1890/15-1928

Ostrofsky, M. L. (2019). Predicting internal phosphorus loading in stratified lakes. *Aquatic Sciences*, *81*(1), 1–9. https://doi.org/10.1007/s00027-018-0618-8

Paludan, C., & Jensen, H. S. (1995). Sequential extraction of phosphorus in freshwater wetland and lake sediment: Significance of humic acids. *Wetlands*, *15*(4), 365–373. https://doi.org/10.1007/BF03160891

Paraska, D. W., Hipsey, M. R., & Ursula Salmon, S. (2014). Sediment diagenesis models: Review of approaches, challenges and opportunities. *Environmental Modelling & Software*, *61*, 297–325. https://doi.org/10.1016/j.envsoft.2014.05.011

Parkhurst, D. L., & Appelo, C. A. J. (2013). Description of input and examples for PHREEQC Version 3—A computer program for speciation batch-reaction, one-dimensional transport, and inverse geochemical calculations. In *U.S. Geological Survey Techniques and Methods* (book 6, chap. A43, 497 p.). https://pubs.usgs.gov/tm/06/a43/

Parsons, C. T., Rezanezhad, F., O'Connell, D. W., & Van Cappellen, P. (2017). Sediment phosphorus speciation and mobility under dynamic redox conditions. *Biogeosciences Discussions*, *14*, 1–36. https://doi.org/10.5194/bg-2016-533

Reitzel, K., Ahlgren, J., DeBrabandere, H., Waldeback, M., Gogoll, A., Tranvik, L., & Rydin, E. (2006). Degradation rates of organic phosphorus in lake sediment. *Biogeochemistry*, *82*(1), 15–28. https://doi.org/10.1007/s10533-006-9049-z

Reitzel, K., Jensen, H. S., & Egemose, S. (2013). pH dependent dissolution of sediment aluminum in six Danish lakes treated with aluminum. *Water research*, *47*(3), 1409–1420. https://doi.org/10.1016/j.watres.2012.12.004

Reynolds, C. S., Irish, A. E., & Elliott, J. A. (2001). The ecological basis for simulating phytoplankton responses to environmental change (PROTECH). *Ecological Modelling*, *140*(3), 271–291. https://doi.org/10.1016/S0304-3800(01)00330-1

Robson, B. J. (2014). State of the art in modelling of phosphorus in aquatic systems: Review, criticisms and commentary. *Environmental Modelling &, Software*, *61*, 339–359. https://doi.org/10.1016/j.envsoft.2014.01.012

Saloranta, T. M., & Andersen, T. (2007). MyLake—A multi-year lake simulation model code suitable for uncertainty and sensitivity analysis simulations. *Ecological Modelling*, *207*(1), 45–60. https://doi.org/10.1016/j.ecolmodel.2007.03.018

Schauser, I., Hupfer, M., & Brüggemann, R. (2006). Sensitivity analysis with a phosphorus diagenesis model (SPIEL). *Ecological Modelling*, *190*, 87–98. https://doi.org/10.1016/j.ecolmodel.2005.03.024

Schmid, M., Hunziker, S., & Wuest, A. (2014). Lake surface temperatures in a changing climate: A global sensitivity analysis. *Climatic Change*, *124*(1-2), 301–315. https://doi.org/10.1007/s10584-014-1087-2

Schmid, M., Ostrovsky, I., & McGinnis, D. F. (2017). Role of gas ebullition in the methane budget of a deep subtropical lake: What can we learn from process-based modeling? *Limnology and Oceanography*, *62*(6), 2674–2698. https://doi.org/10.1002/lno.10598

Schutz, J., Rydin, E., & Huser, B. J. (2017). A newly developed injection method for aluminum treatment in eutrophic lakes: Effects on water quality and phosphorus binding efficiency. *Lake and Reservoir Management*, *33*(2), 152–162. https://doi.org/10.1080/10402381.2017.1318418

Shimoda, Y., Ekram Azim, M., Perhar, G., Ramin, M., Kenney, M. A., Sadraddini, S., et al. (2011). Our current understanding of lake ecosystem response to climate change: What have we really learned from the north temperate deep lakes? *Journal of Great Lakes Research*, *37*(1), 173–193. https://doi.org/10.1016/j.jglr.2010.10.004

Skarbøvik, E., Haande, S., Bechmann, B., & Skjelbred, M. (2019). Monitoring Morsa 2017-2018 (in Norwegian). *NIBIO*, *5*(30/2019), 64.

Smith, V. H., Tilman, G. D., & Nekola, J. C. (1999). Eutrophication: Impacts of excess nutrient inputs on freshwater, marine, and terrestrial ecosystems. *Environmental Pollution*, *100*(1-3), 179–196.

Smits, J. G. C., & van Beek, J. K. L. (2013). ECO: a generic eutrophication model including comprehensive sediment-water interaction. *PloS One*, *8*(7), e68104. https://doi.org/10.1371/journal.pone.0068104

Smolders, A. J. P., Lamers, L. P. M., Lucassen, E. C. H. E., Van Der Velde, G., & Roelofs, J. G. M. (2006). Internal eutrophication: How it works and what to do about it—A review. *Chemistry and Ecology*, *22*(2), 93–111. https://doi.org/10.1080/02757540600579730

Soetaert, K., Middelburg, J. J., Herman, P. M. J., & Buis, K. (2000). On the coupling of benthic and pelagic biogeochemical models. *Earth-Science Reviews*, *51*(1-4), 173–201. https://doi.org/10.1016/s0012-8252(00)00004-0

Solheim, A. L., Rohrlack, T., Grung, M., Hobæk, A., Bennion, H., Burgess, A., & Yang, H. (2006). Study on reference condition and development of eutrophication in lake vansjø, (in norwegian). *NIVA report*, 5145–2006. http://hdl.handle.net/11250/213072. ISBN 82-577-4858-7

Stefan, H. G., Fang, X., & Eaton, J. G. (2001). Simulated fish habitat changes in North American lakes in response to projected climate warming. *Transactions of the American Fisheries Society*, *130*(3), 459–477. https://doi.org/10.1577/1548-8659 (2001)130<0459:sfhcin>2.0.co;2

Testa, J. M., Brady, D. C., Di Toro, D. M., Boynton, W. R., Cornwell, J. C., & Kemp, W. M. (2013). Sediment flux modeling: Simulating nitrogen, phosphorus, and silica cycles, Estuarine. *Coastal and Shelf Science*, *131*(c), 245–263. https://doi.org/10.1016/j.ecss.2013.06.014

Tranvik, L. J., Cotner, J. B., Loiselle, S. A., Striegl, R. G., Ballatore, T. J., Dillon, P., et al. (2009). Lakes and reservoirs as regulators of carbon cycling and climate. *Limnology and Oceanography*, *54*(6part2), 2298–2314. https://doi.org/10.4319/lo.2009.54.6_part_2.2298

Trolle, D., Hamilton, D. P., Pilditch, C. A., Duggan, I. C., & Jeppesen, E. (2011). Predicting the effects of climate change on trophic status of three morphologically varying lakes: Implications for lake restoration and management. *Environmental Modelling &, Software*, *26*(4), 354–370. https://doi.org/10.1016/j.envsoft.2010.08.009

Trolle, D., Skovgaard, H., & Jeppesen, E. (2008). The water framework directive: Setting the phosphorus loading target for a deep lake in Denmark using the 1D lake ecosystem model DYRESM–CAEDYM. *Ecological Modelling*, *219*(1-2), 138–152. https://doi.org/10.1016/j.ecolmodel.2008.08.005

Van Cappellen, P., & Wang, Y. (1996). Cycling of iron and manganese in surface sediments; a general theory for the coupled transport and reaction of carbon, oxygen, nitrogen, sulfur, iron, and manganese. *American Journal of Science*, *296*(3), 197–243. https://doi.org/10.2475/ajs.296.3.197

Verschoor, M. J., Powe, C. R., McQuay, E., Schiff, S. L., Venkiteswaran, J. J., Li, J., & Molot, L. A. (2017). Internal iron loading and warm temperatures are preconditions for cyanobacterial dominance in embayments along Georgian Bay, Great Lakes. *Canadian Journal of Fisheries and Aquatic Sciences*, *74*, 1–15. https://doi.org/10.1139/cjfas-2016-0377

Visser, P. M., Verspagen, J. M. H., Sandrini, G., Stal, L. J., Matthijs, H. C. P., Davis, T. W., et al. (2016). How rising CO and global warming may stimulate harmful cyanobacterial blooms. *Harmful Algae*, *54*, 145–159. https://doi.org/10.1016/j.hal.2015.12.006

Warszawski, L., Frieler, K., Huber, V., Piontek, F., Serdeczny, O., & Schewe, J. (2014). The Inter-Sectoral Impact Model Intercomparison Project (ISI-MIP): Project framework. *Proceedings of the National Academy of Sciences of the United States of America*, *111*(9), 3228–3232. https://doi.org/10.1073/pnas.1312330110

Wilfert, P., Kumar, P. S., Korving, L., Witkamp, G.-J., & van Loosdrecht, M. C. M. (2015). The relevance of phosphorus and iron chemistry to the recovery of phosphorus from wastewater: A review. *Environmental Science & Technology*, *49*(16), 9400–9414. https://doi.org/10.1021/acs.est.5b00150

Winder, M., & Sommer, U. (2012). Phytoplankton response to a changing climate. *Hydrobiologia*, *698*(1), 5–16. https://doi.org/10.1007/s10750-012-1149-2

Winslow, L. A., Leach, T. H., & Rose, K. C. (2018). Global lake response to the recent warming hiatus. *Environmental Research Letters*, *13*(5), 054005. https://doi.org/10.1088/1748-9326/aab9d7

Woolway, R. I., & Merchant, C. J. (2019). Worldwide alteration of lake mixing regimes in response to climate change. *Nature Geoscience*, *12*(4), 271–276. https://doi.org/10.1038/s41561-019-0322-x

Xiong, Y., Guilbaud, R., Peacock, C. L., Cox, R. P., Canfield, D. E., Krom, M. D., & Poulton, S. W. (2019). Phosphorus cycling in Lake Cadagno Switzerland: A low sulfate euxinic ocean analogue. *Geochimica et Cosmochimica Acta*, *251*, 116–135. https://doi.org/10.1016/j.gca.2019.02.011

Yvon-Durocher, G., Caffrey, J. M., Cescatti, A., Dossena, M., del Giorgio, P., Gasol, J. M., et al. (2012). Reconciling the temperature dependence of respiration across timescales and ecosystem types. *Nature*, *487*(7408), 472–476. https://doi.org/10.1038/nature11205

Zhang, Z., Sun, B., & Johnson, B. E. (2015). Integration of a benthic sediment diagenesis module into the two dimensional hydrodynamic and water quality model—CE-QUAL-W2. *Ecological Modelling*, *297*, 213–231. https://doi.org/10.1016/j.ecolmodel.2014.10.025

Erratum

In the originally published version of this article, the list of author contributions was incomplete. The Author Contributions have since been corrected, and this version may be considered the authoritative version of record.